Applications of X-ray Imaging in Bio-medical and Material Science research

Giuliana Tromba
Sincrotrone Trieste

Outline

- **SR-based X-ray imaging techniques**

  - k-edge absorption imaging

  - phase sensitive imaging techniques:

  PHase Contrast radiography

  Diffraction Enhanced Imaging (DEI)

- **Applications at the SYRMEP beamline**

Main advantages in the use of SR

- Monochromaticity -> no beam hardening
  k-edge imaging
  quantitative evaluations
  optimization of X-ray energy with sample characteristics (dose reduction)
- Collimation -> parallel beams, scatter reduction
- Spatial coherence -> phase sensitive techniques
- High intensity -> reduction of exposure time

K-edge Subtraction Imaging

1. Contrast agent injection: Iodine (or Gadolinium)
2. Two Images are acquired : Above (A) and Below (B) the K-edge
3. Image processing : Iodine and Tissue images

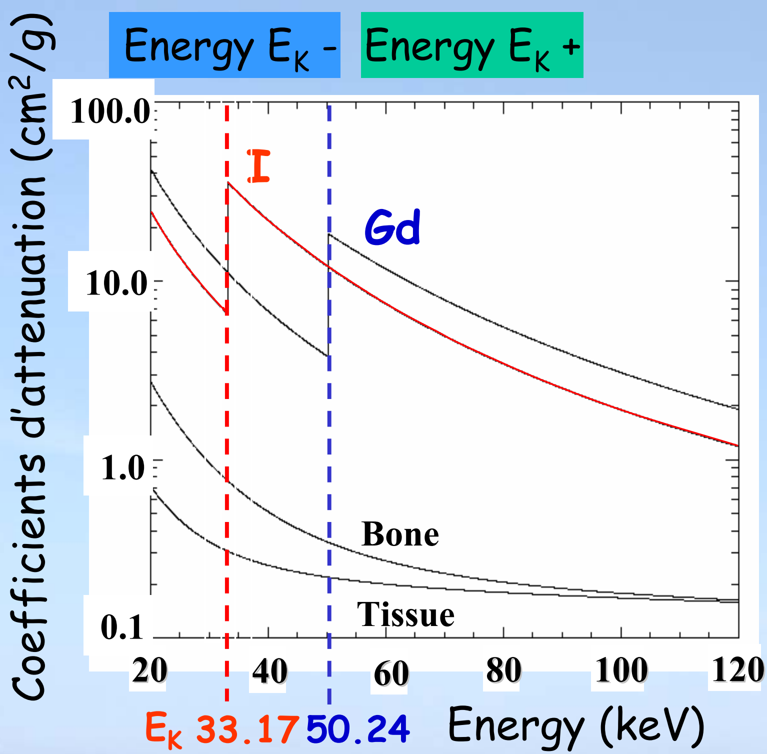

$$x_i = \frac{\mu_{Bi} \ln(A) - \mu_{Ai} \ln(B)}{\mu_{Bi}\mu_{At} - \mu_{Ai}\mu_{Bt}}$$

$$x_t = \frac{\mu_{Bi} \ln(A) - \mu_{Ai} \ln(B)}{\mu_{Bi}\mu_{At} + \mu_{Ai}\mu_{Bt}}$$

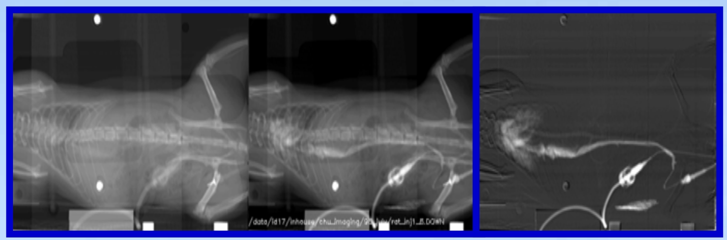

Below   Above K-edge   Iodine Image

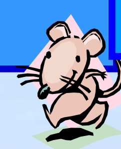

Courtesy of A.Bravin (ESRF)

Phase-sensitive imaging techniques

Conventional radiology relies on X-ray absorption as the unique source of contrast and is based exclusively on the detection of amplitude variation of the transmitted X-rays.
Main limitation ⟶ poor contrast for samples with low-Z composition.

Phase sensitive imaging techniques are based on the observation of the *phase shifts* produced by the object on the incoming wave.

Refractive index: $n = 1 - \delta + i\,\beta$
β = absorption term; δ = phase shift term
$\beta \sim 10^{-10}$; $\delta \sim 10^{-6}$ in soft tissue @ 17 keV
$\delta \propto \lambda^2$, $\beta \propto \lambda^3$
Absorption radiology -> contrast generated by differences in the x-ray absorption ($\beta\,\Delta z$)
Phase Radiology –> contrast generated by phase shifts x-ray absorption ($\delta\,\Delta z$)
($\delta >> \beta$ –> phase contrast >> absorption contrast

PHase-Contrast radiography (PHC)

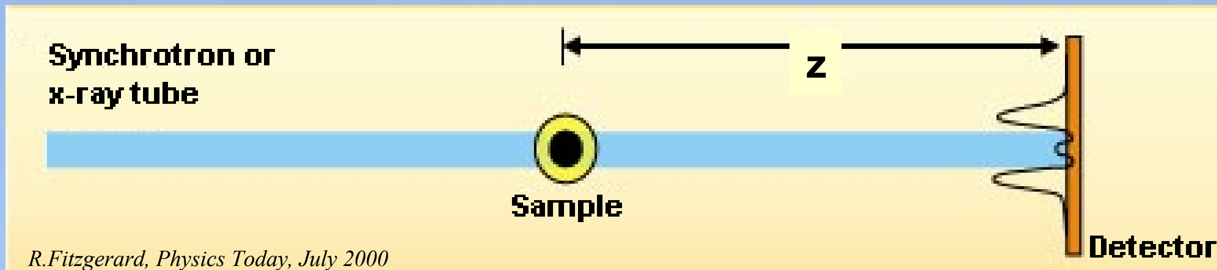

R.Fitzgerard, Physics Today, July 2000

- Similar to technique for in-line holography by D.Gabor (1948), first implementation with a conventional source was by Davis et al. (Nature 373, 1995) and with SR by A.Snigirev et al. *(Rev.Sci.Instrum., 66, 1995).* F.Arfelli et al. (Phys.Med.Biol. 43, 1998) implemented it for medical imaging.
- The technique exploits the high spatial coherence of the X-ray source.
- z =0 -> absorption image
- For z > 0 -> interference between diffracted and un-diffracted wave produces edge and contrast enhancement. A variation of δ is detected
- Measure of $\nabla^2\Phi(x,y)$

Regimes

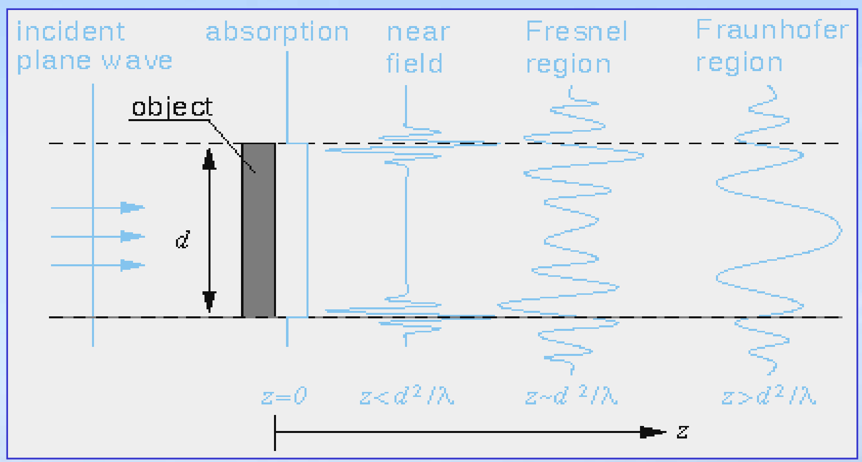

Simulated PHC patterns for a 100 μm nylon wire

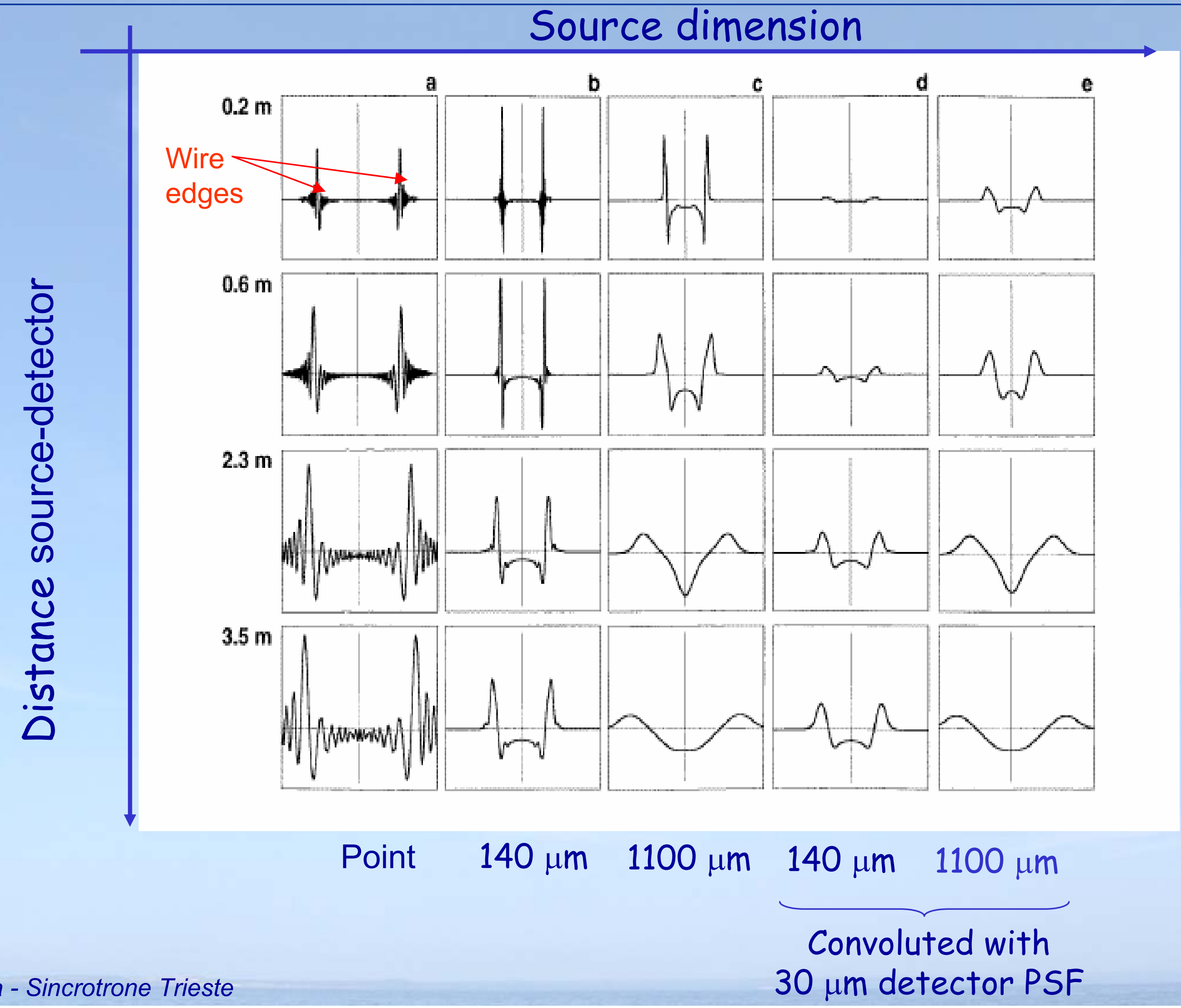

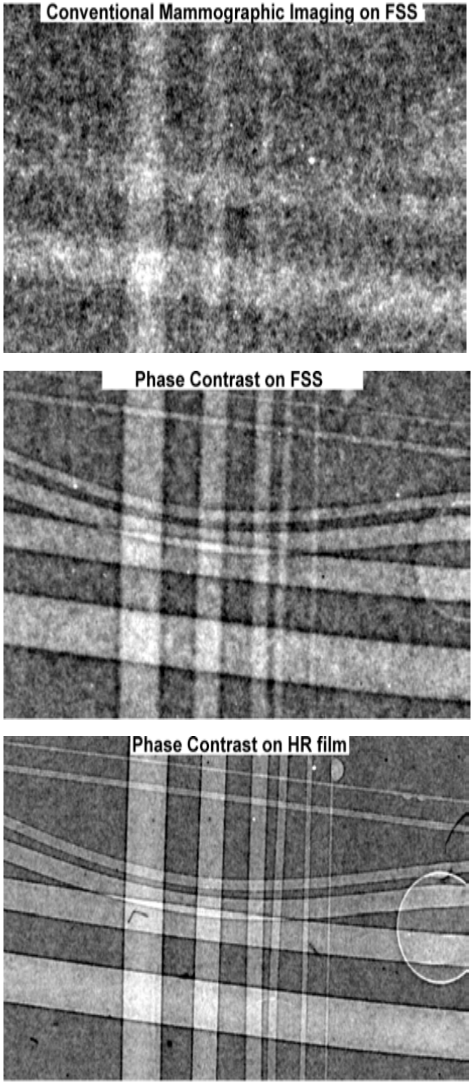

Real images
of nylon wires

Diffraction Enhanced Imaging (DEI)

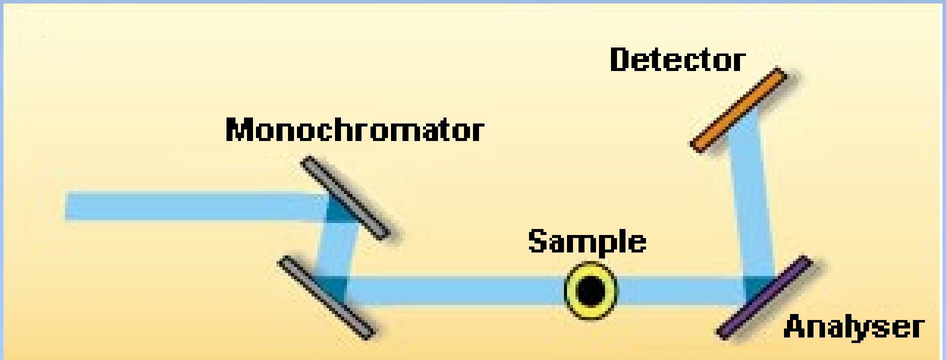

R.Fitzgerard, Physics Today, July 2000

- The technique was first explored by K.M. Podurets et al. (Sov. Phys. Tech. Phys. 34(6), June 1989) and by Ingal et al. (App. Phys. 28, 1995) with different names as “refraction-contrast radiography”, “phase dispertion introscopy”. First physics interpretation by D.Chapman et al., Phys.Med.Biol. 42, 1997.
- A perfect crystal is used as an angular filter to select angular emission of X-rays. The filtering function is the rocking curve (FWHM: 1-20 μrad)
- Analyzer and monochromator aligned -> X-ray scattered by more than some tens μrad are rejected
- Small misalignements -> investigation of phase shift effects (refraction angle is roughly proportional to the gradient of δ)
- With greater misalignements the primary beam is almost totally rejected and pure refraction images are obtained
- $\nabla\Phi(x,y)$

Extinction and Refraction Contrast

- The analyzer crystal acts as an angular band-pass filter:
  - Photons deviated outside the rocking curve width are not diffracted by the analyzer towards the detector
    - » Extinction contrast
  - Photons deviated within the rocking curve width are diffracted by the analyzer towards the detector, the probability being modulated by the rocking curve
    - » Refraction contrast

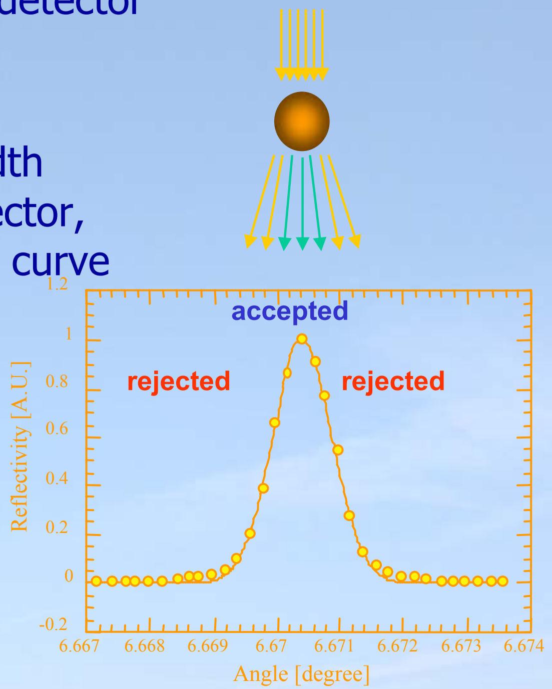

Extinction and refraction contrast depend on the position of the analyzer on the rocking curve

Principles of DEI – basic algorithm

- Components of a X-ray radiograph:
  - Coherent scattering (I_{CS});
  - Incoherent scattering (I_{IS});
  - Transmitted beam (I_T)

I_T is affected by diffraction of organized structures inside the sample (SAXS) (I_{SAXS}) and by refraction (I_R) and attenuated by absorption and extinction.

Image formation in a conventional radiograph -> $I = I_{CS} + I_{IS} + I_{SAXS} + I_R$

DEI allows to separate I_R from the other components and to obtain two images:

-Refracted image

-Apparent absorption image (absorption + extinction)

Main limitation:
Does not distinguish refraction from USAXS (ultra-small angle scattering produced by very small unresolved structure)

Refraction

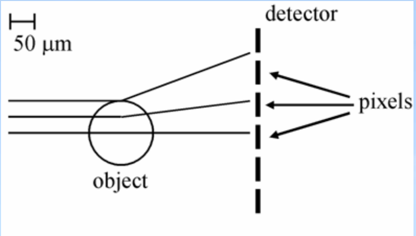

USAXS

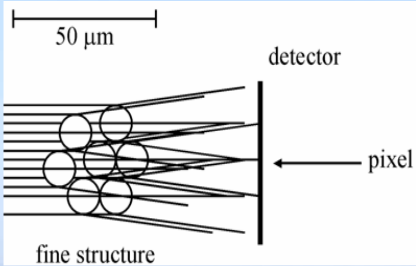

Analyzer Tuning

Top ($\theta=\theta_B$)

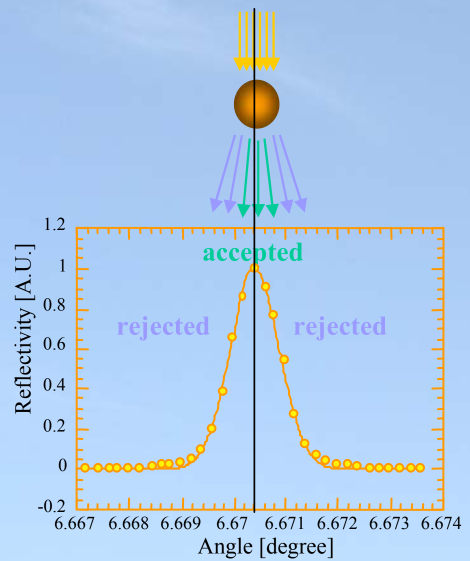

$R(\theta_B + \Delta\theta(x,y)) < R(\theta_B)$

Slope ($\theta\neq\theta_B$)

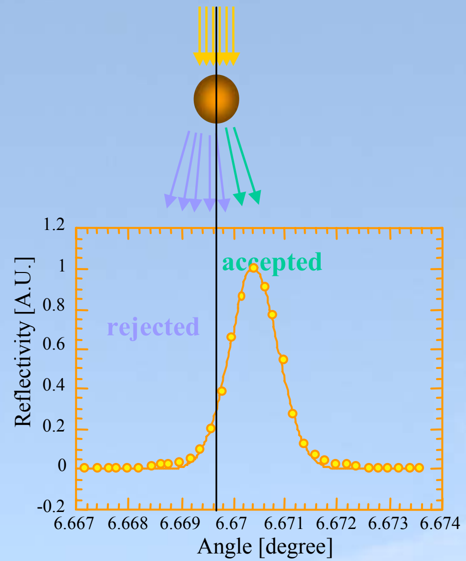

$R(\theta+\Delta\theta(x,y)) \lesseqgtr R(\theta)$

- $\Delta\theta(x,y)$ ~ Rocking Curve Width => Refraction Contrast
- $\Delta\theta(x,y)$ >> Rocking Curve Width (SAXS) => Extinction Contrast

DEI image manipulation

I_L

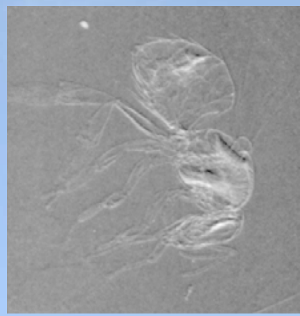

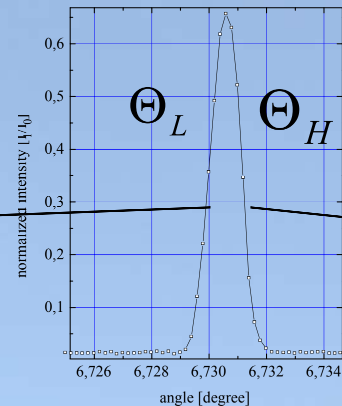

I_H

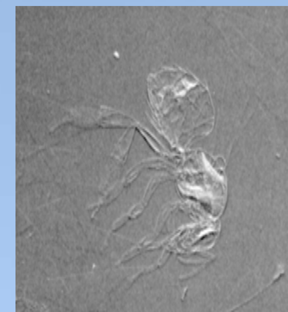

$$I_L = I_R\left(R(\Theta_L) + \frac{\partial R}{\partial \Theta}(\Theta_L)\Delta\Theta_z \right)$$

$$I_H = I_R\left(R(\Theta_H) + \frac{\partial R}{\partial \Theta}(\Theta_H)\Delta\Theta_z \right)$$

Θ_Z = refraction Image

I_R = apparent absorption image (absorption+extinction)

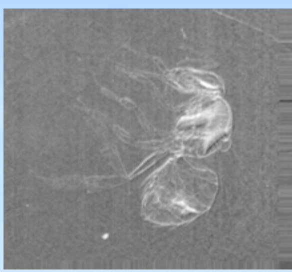

Apparent Absorption Image

$$I_R = \frac{I_L \cdot \left.\frac{dR}{d\Theta}\right|_{\Theta_H} - I_H \cdot \left.\frac{dR}{d\Theta}\right|_{\Theta_L}}{R(\Theta_L)\cdot \left.\frac{dR}{d\Theta}\right|_{\Theta_H} - R(\Theta_H)\cdot \left.\frac{dR}{d\Theta}\right|_{\Theta_L}}$$

$$\Theta_Z = \frac{I_H \cdot R(\Theta_L) - I_L \cdot R(\Theta_H)}{I_L \cdot \left.\frac{dR}{d\Theta}\right|_{\Theta_H} - I_H \cdot \left.\frac{dR}{d\Theta}\right|_{\Theta_L}}$$

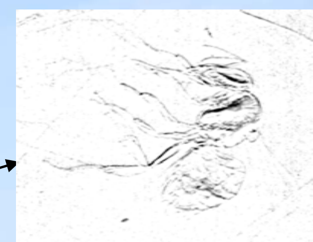

Refraction Image

Ref: Chapman et al, Phys.Med.Biol, 42,1997

SYRMEP layout for PHC imaging

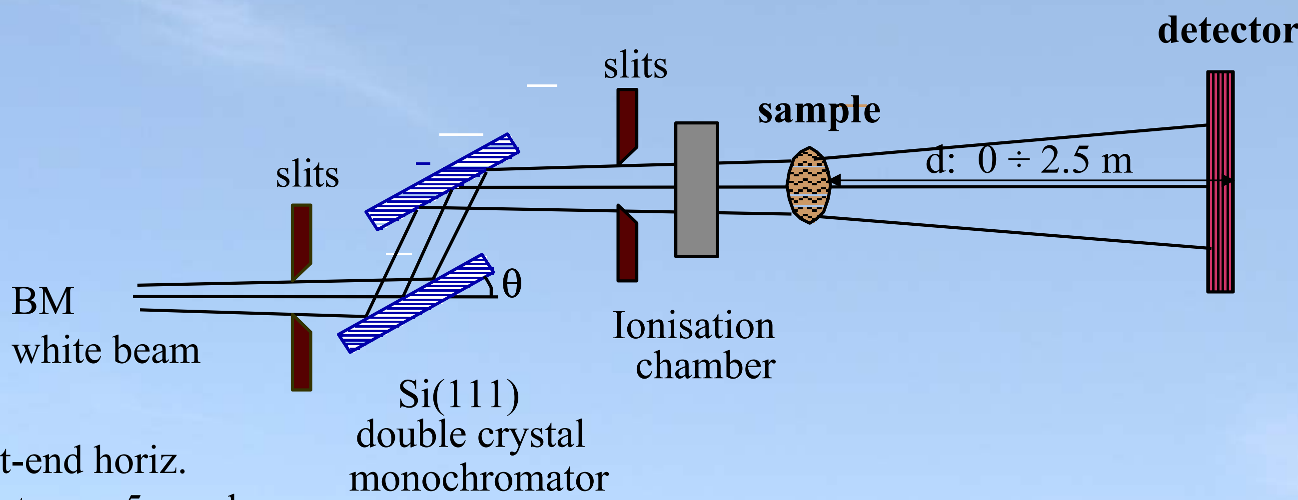

Front-end horiz.
acceptance: 5 mrad

SYRMEP beamline setup for DEI

Sources of contrast: absorption, extinction and refraction

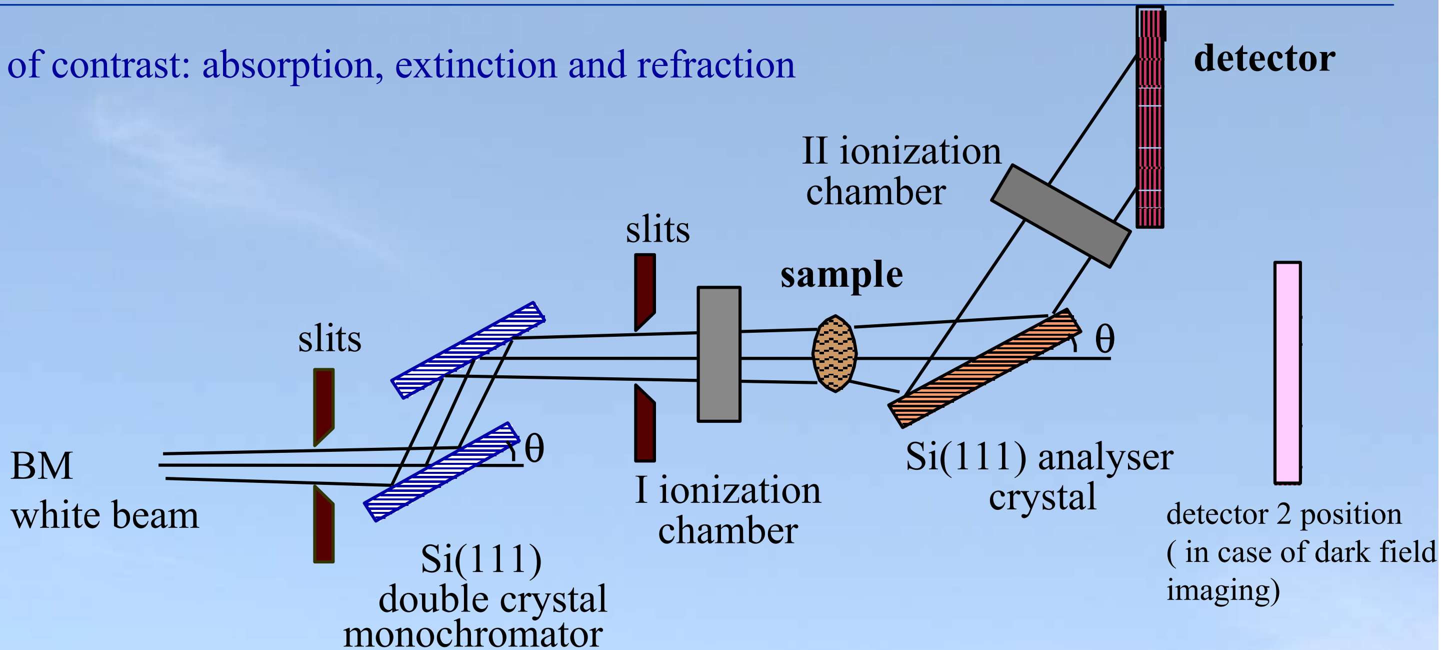

Refractive index $n = 1 - \delta + i\beta$

Variation of δ in the sample => Photons are refracted at μrad angles

- The analyzer crystal acts as a angular filter: filtering function is the rocking curve (FWHM: 1-20 μrad)
- Photons deviated outside the rocking curve width are not detected
- Photons deviated within the rocking curve width are diffracted towards the detector (probability modulated by the rocking curve)

Two ionization chambers allow to set the analyzer crystal on a certain position of the rocking curve

DEI Set-up

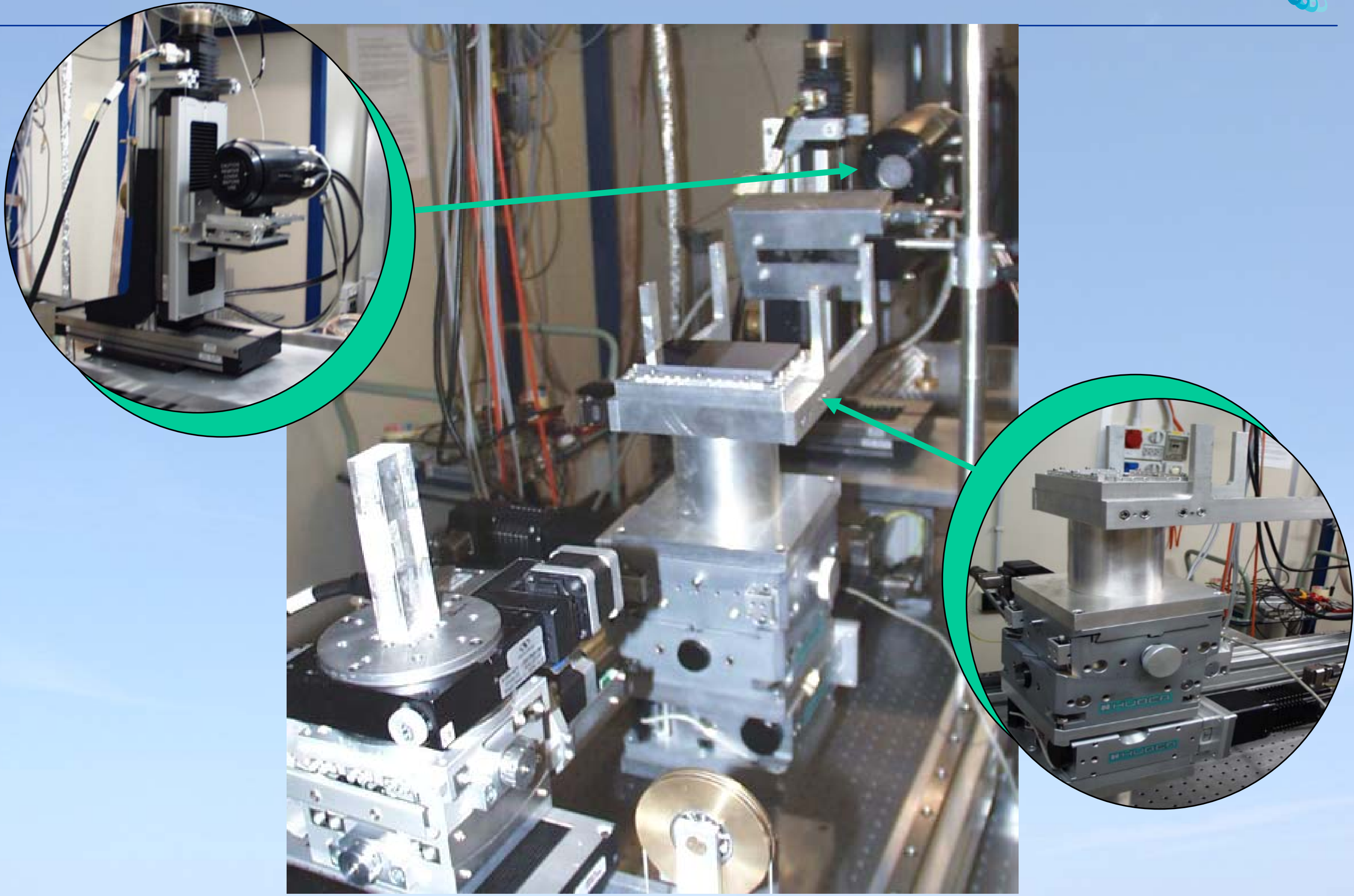

The SYRMEP beamline

Source Characteristics

- Source size ≅ 100 µm x 1100 µm
- Source-to-sample distance ≅ 23 m
- Sample-to-detector distance d: 0 ÷ 2.5 m
- Energy range: 8 ÷ 35 keV, Bandwidth $\Delta E/E \cong 10^{-3}$
- Typical fluxes at 15 keV ≅ $2 \cdot 10^8$ phot./mm^2 s (@ 2 GeV, 300 mA)
  $7 \cdot 10^8$ phot./mm^2 s (@ 2.4 GeV, 180 mA)
- Transverse coherence length at 15 keV ($L_c = \lambda L / 2*\sigma$) ≅ 10 µm

Detectors

- High Resolution films (1 µm resolution)
- Medical screen-film systems (≅ 35 µm resolution)
- CCD (2048*2048 pixels) with 2 configurations:
  - pixel size: 14 µm, 1:1 optical fiber taper, field of view: 28.67x28.67 mm^2
  - pixel size: about 5 µm, with 11:40 magnifying optics, field of view of about 8mm^2.
- CCD (4008*2672 pixels), pixel size: 4.5 µm, 1:2 magn. optics, field of view: 18.04 x 12.02 mm^2
- Imaging Plate (IP reader FLA 7000 -25 µm resolution)

PHC vs. Absorption

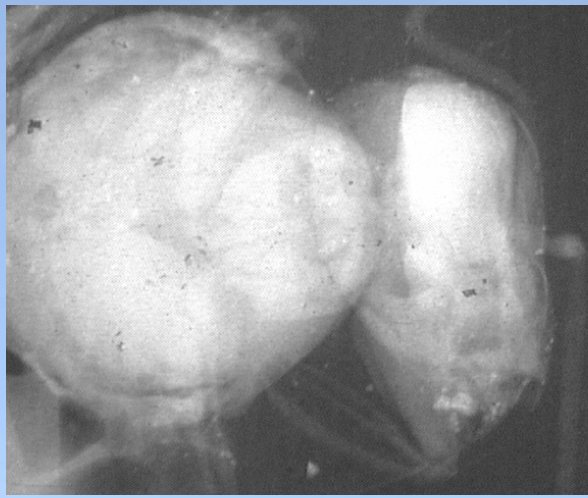

10 keV

Absorption

Phase Contrast

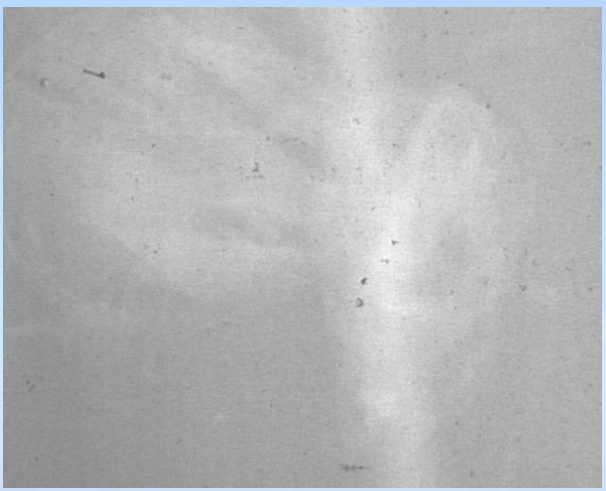

20 keV

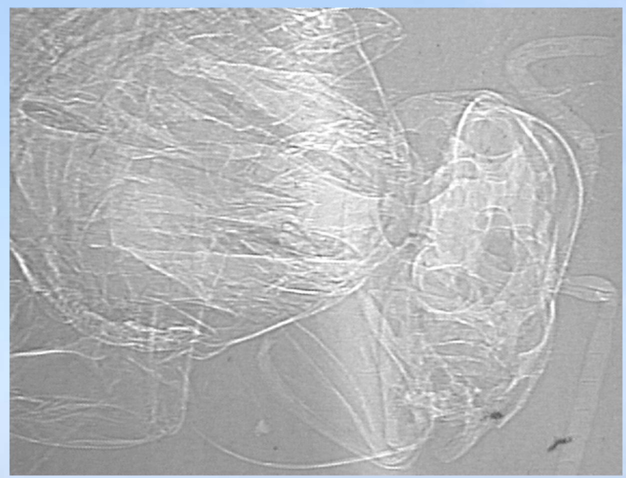

One example of image manipulation with DEI

Apparent absorption

Refraction image

DEI – images at two positions of the rocking curve

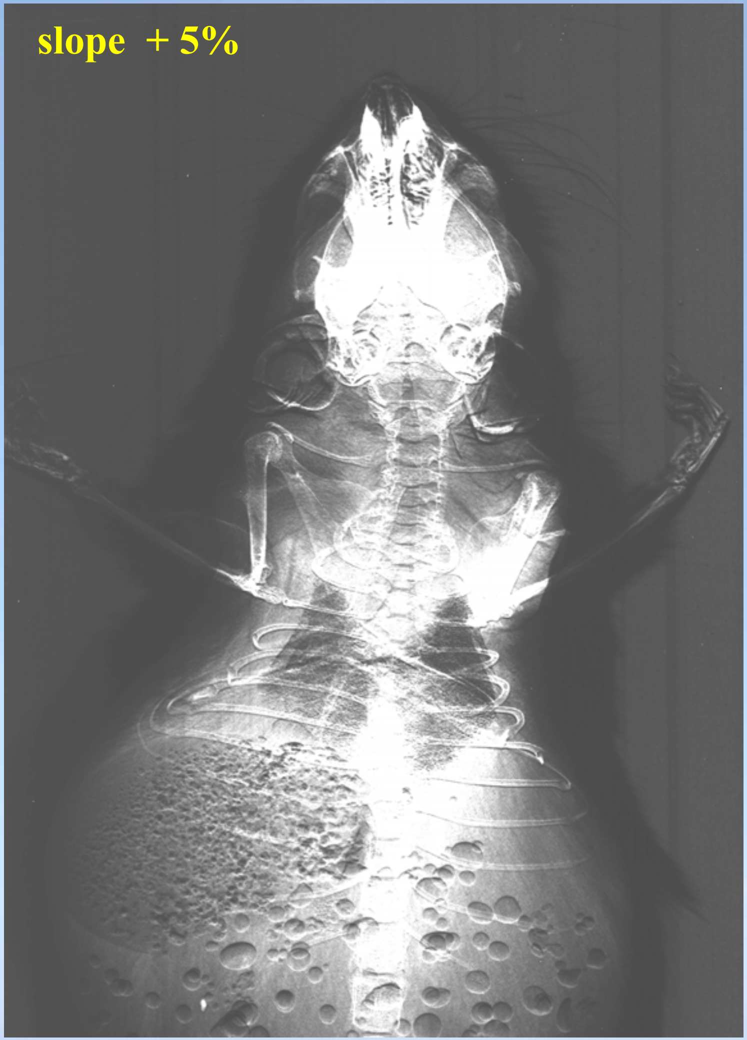

Applications at the SYRMEP beamline

- Imaging of soft tissues and mammography (PHC) -> SYRMA project
- Study of joints and cartilages (DEI)
- Imaging of lungs (DEI)
- Trabecular bone architecture (absorption tomo)
- Study of dental implants (absorption tomo)
- Mapping of the metal intake (PHC and K-edge imaging)
- Imaging of archeological glasses (PHC tomo)
- Study of waterlogged archeological wood (PHC and absorption tomo)

Breast imaging

- Breast cancer is the most common cancer amongst women (incidence: 8%)
- The success of treatment depends on early detection (asynthomatic women)
- Main method for detecting early breast -> **X-ray mammography**
- Screening programs for large population area above 50 years old
- Sensitivity of conventional mammography: 85-90%, Specificity: 90%
- False positive/true positive ≈ 5 -10%
- High number of doubtful cases makes frequent the need of biopsies
- Conventional mammography is **not enough effective** for dense breasts

Radiographs of breasts with increasing density: mainly adipose breast (left) up to high fibro-glandularity breast (right)

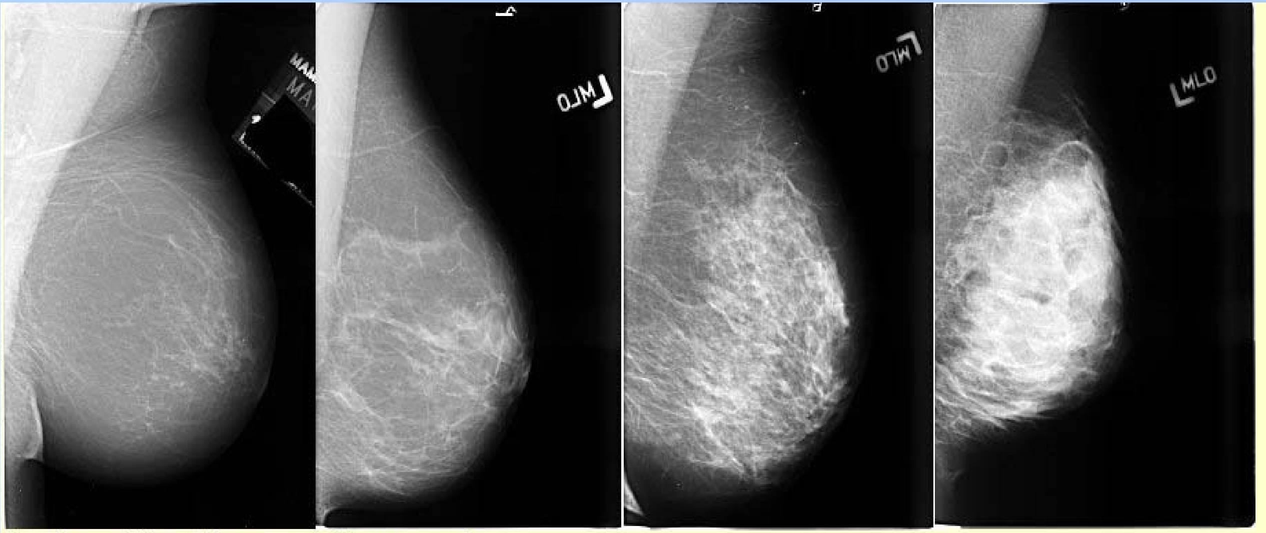

Breast composition and its mammographic appearance.[1]

PHC application to mammography: Human tissue sample

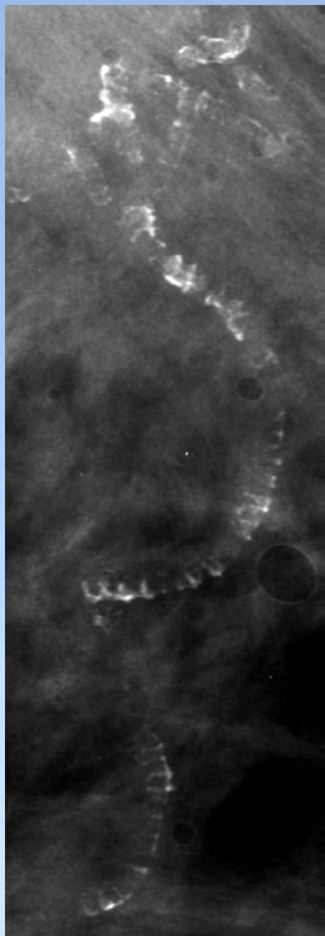

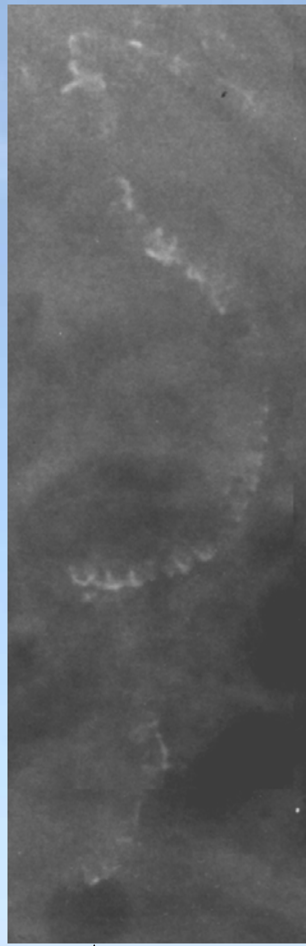

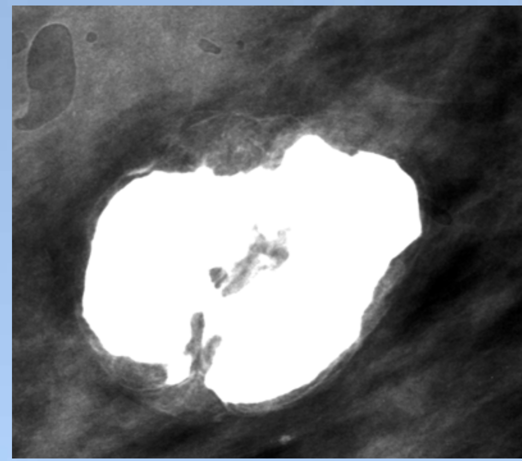

SR

E = 17 keV

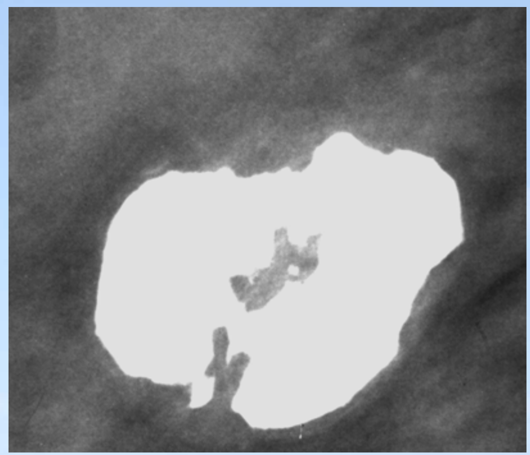

Thickness = 4 cm
MGD = 1.5 mGy

E = 17 keV SR

Conventional X-ray generator

30 kVp, 50 mAs

The SYRMA project
(**SY**nchrotron **R**adiation for **Ma**mmography)

Agreement among the Public Hospital of Trieste, the University of Trieste and Elettra

Aim -> *In vivo* mammography studies on limiterd number of cases selected by the Radiologist;

Target-> Dense breasts;

conventional radiographs with uncertain diagnosis;

suspect of false positives.

Set-ups-> I Phase: PHC planar radiography with conventional screen-film system;

II Phase: implementation of digital detectors;

II Phase: application of tomography and tomosynthesis.

The SYRMA beamline

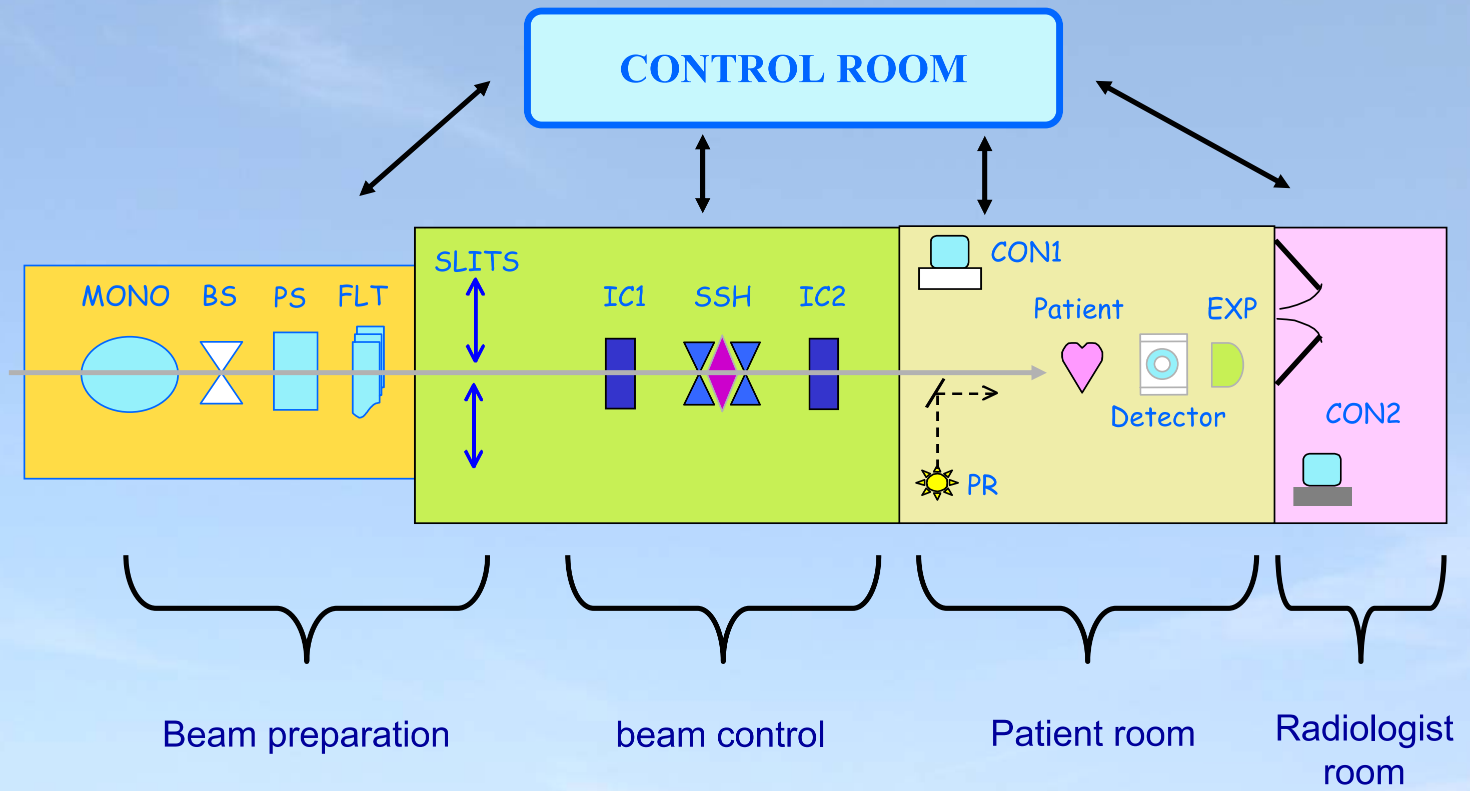

The building

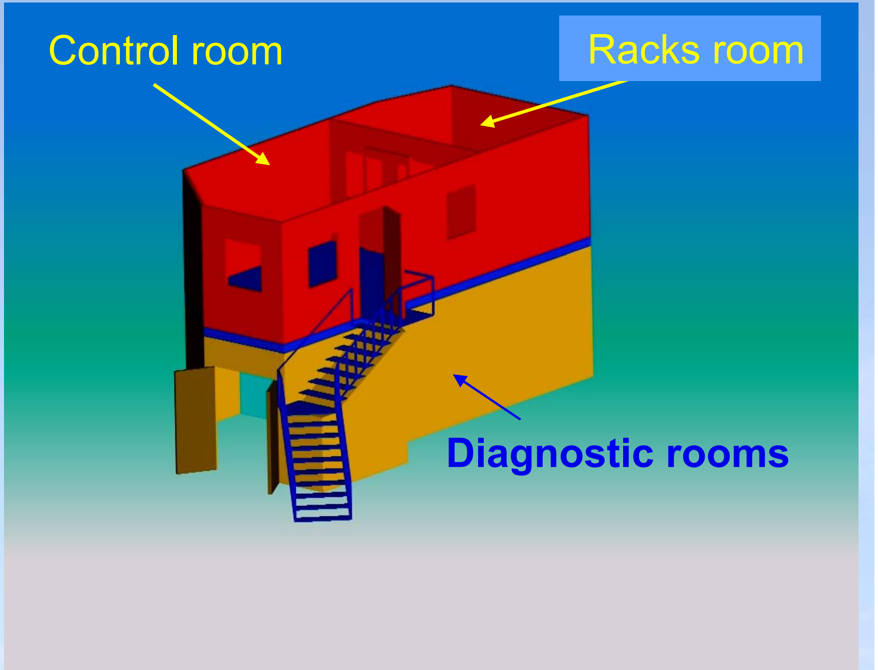

Radiologist room

Patient positioning

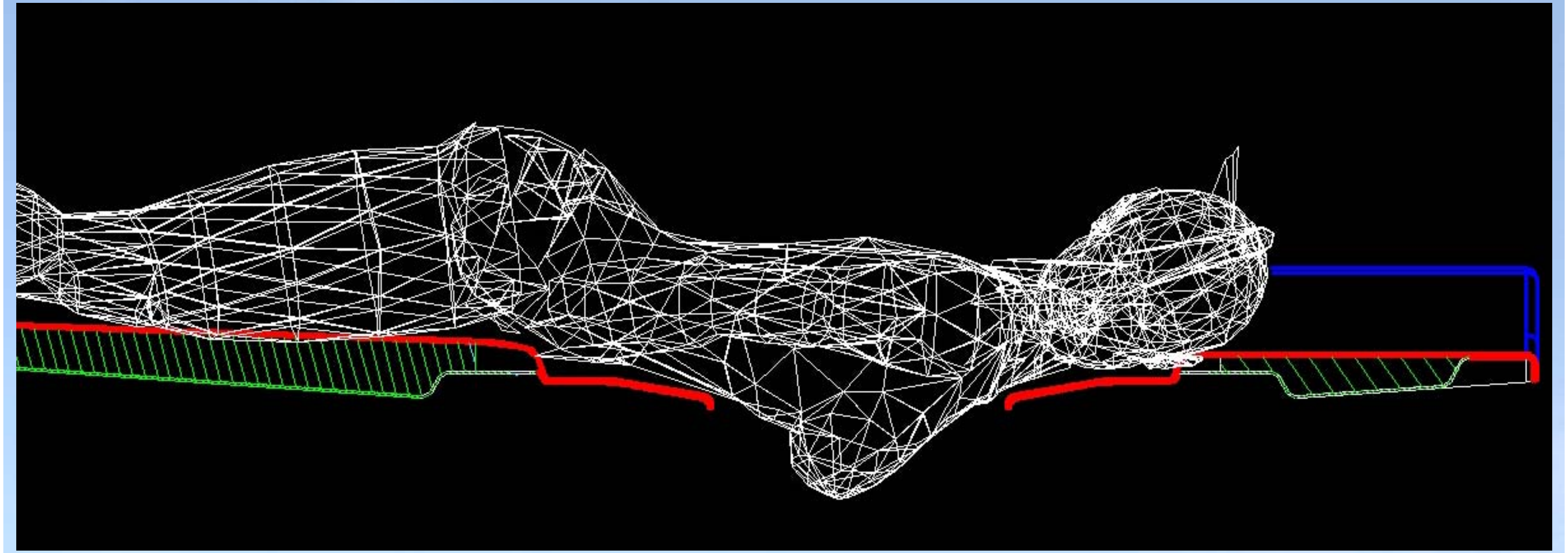

Patient room

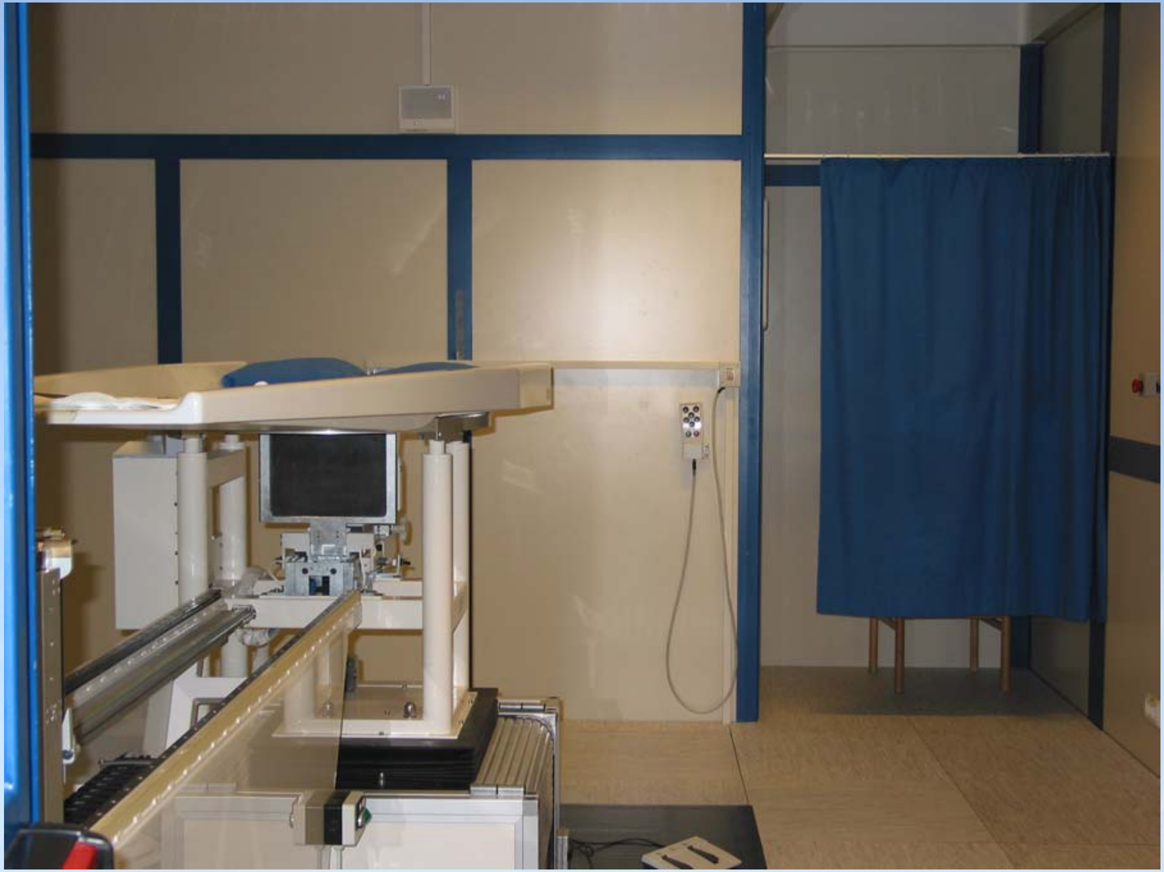

Patient support

Detector holder

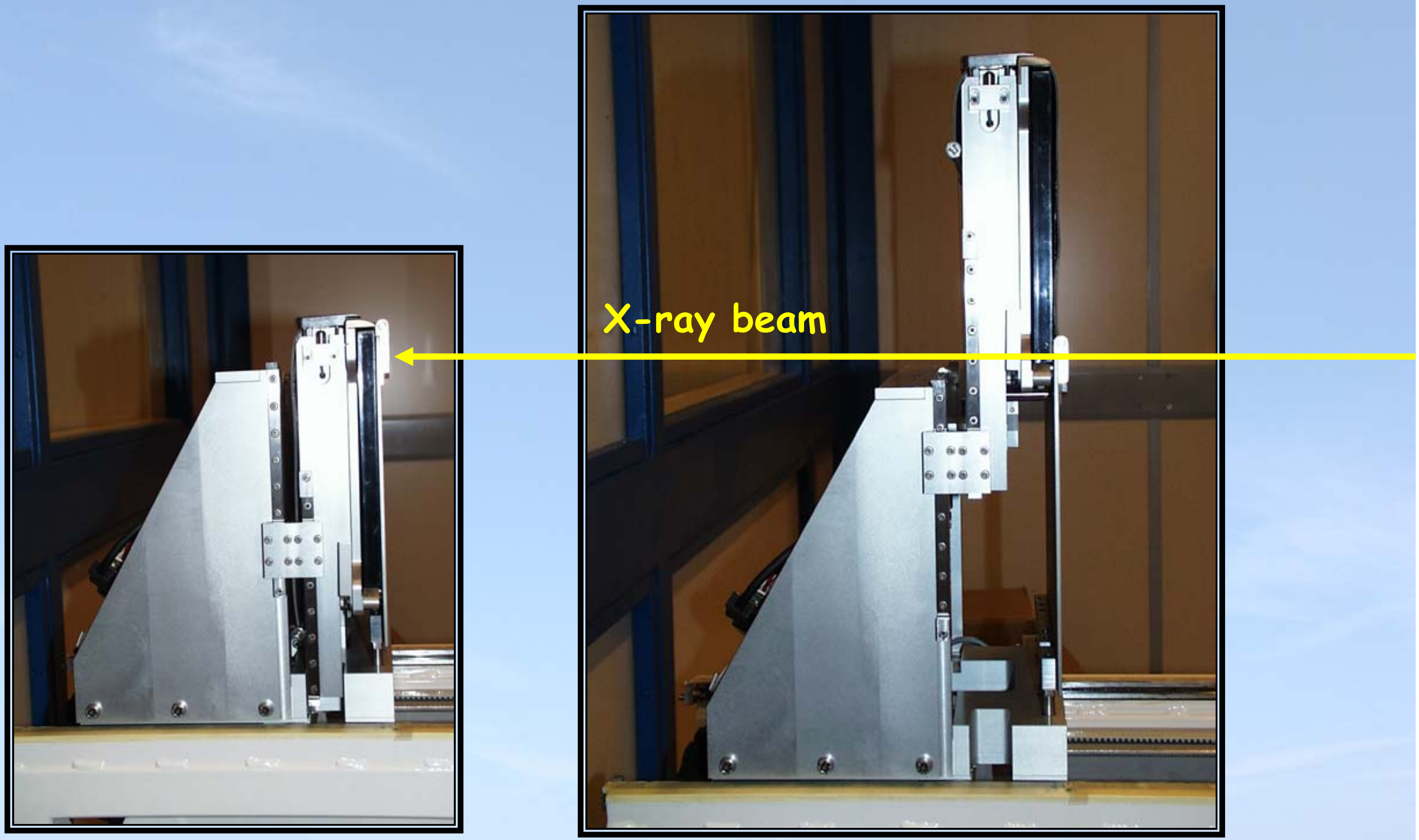

Lungs imaging with DEI

The potential of DEI technique is under evaluation in different contexts :

- cancer detection
- asthma
- pulmonary emphysema

Problems

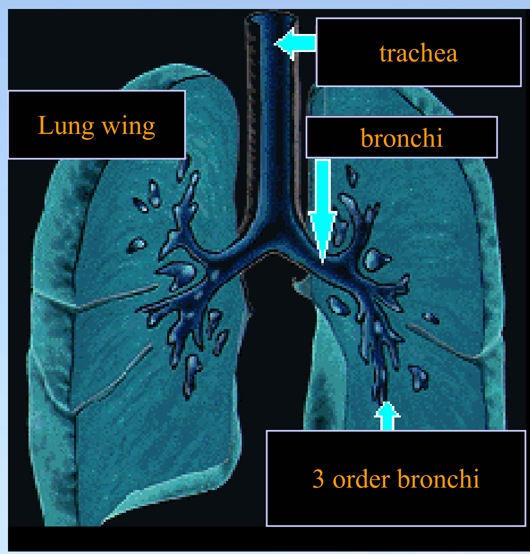

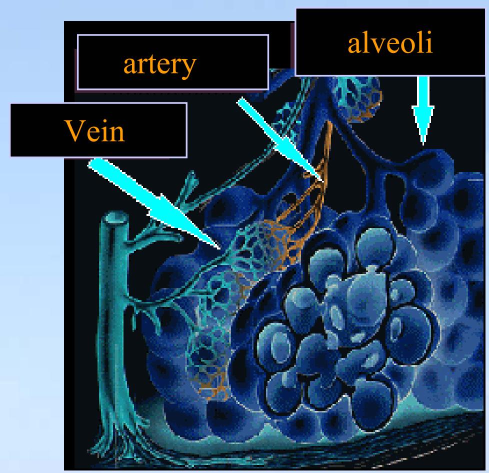

Mouse lungs

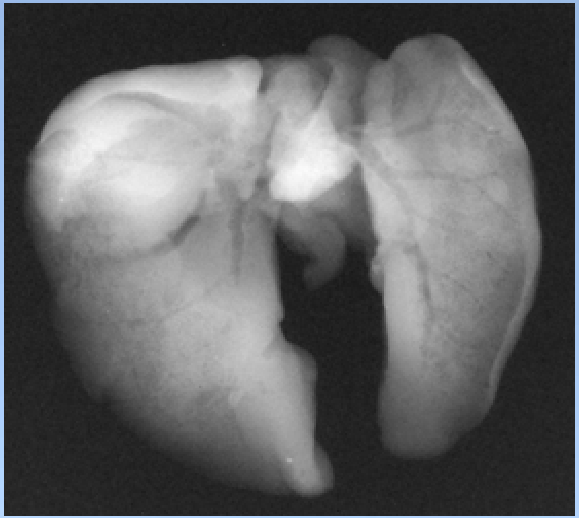

Transmission image

Apparent absorption image

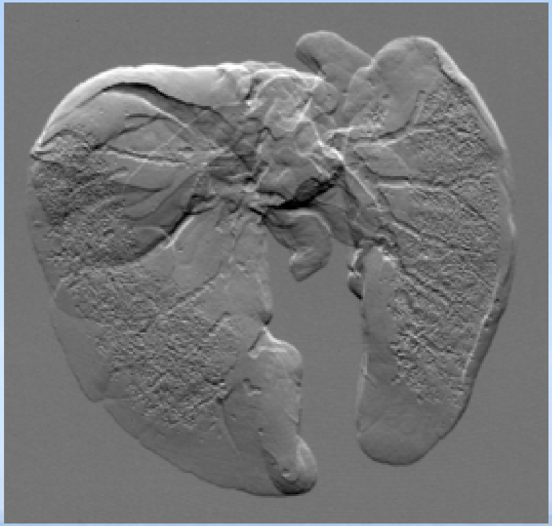

Refraction image

Images at 17 keV

Daresbury, Elettra, University of Trieste Collaboration within PHASY project: R. Lewis, C. Hall, et Al.

Mouse lungs

Top image

Images at 17 keV

Far slope image

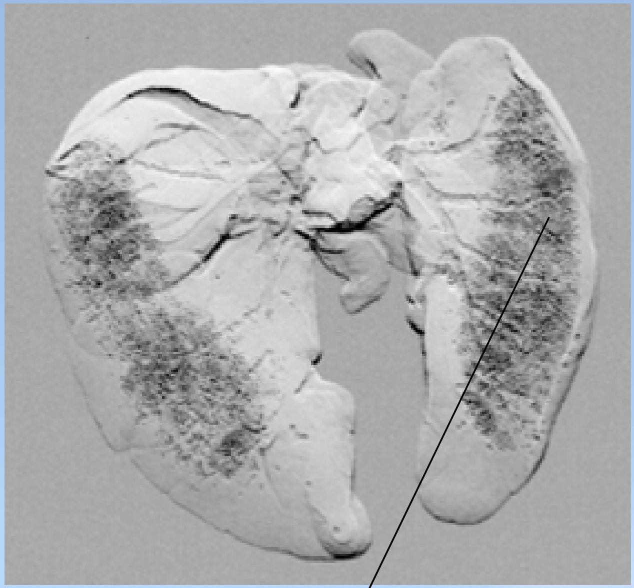

Zoom of top
extinction contrast

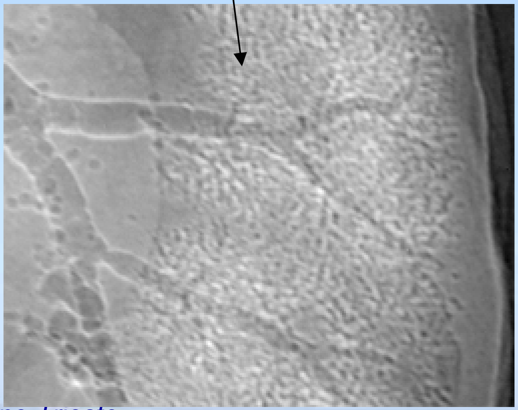

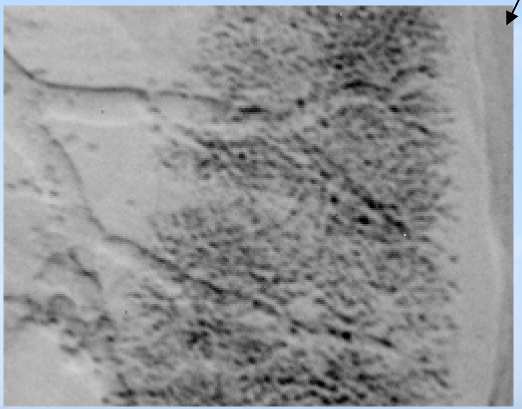

Zoom of far slope
reverse contrast

Finger Joint

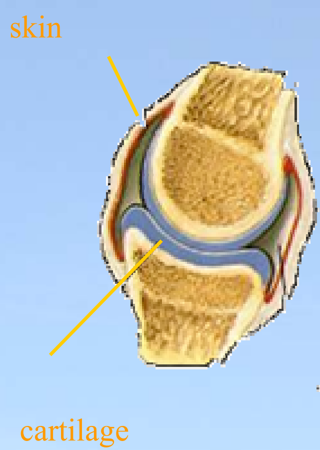

Conventional radiograph

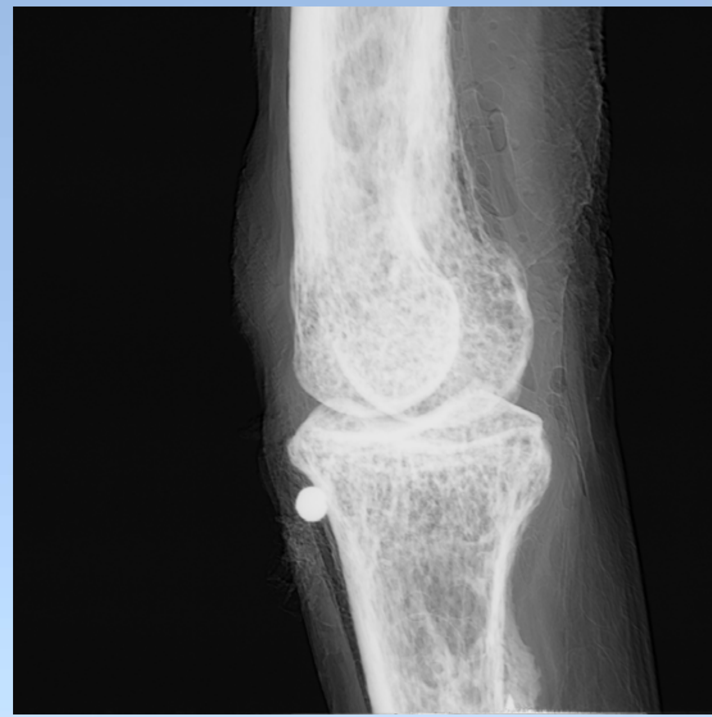

Apparent absorption image @ 20 keV at ELETTRA

Daresbury, Elettra, University of Trieste Collaboration within PHASY project: R. Lewis et al.

Index finger proximal interphalangeal joint

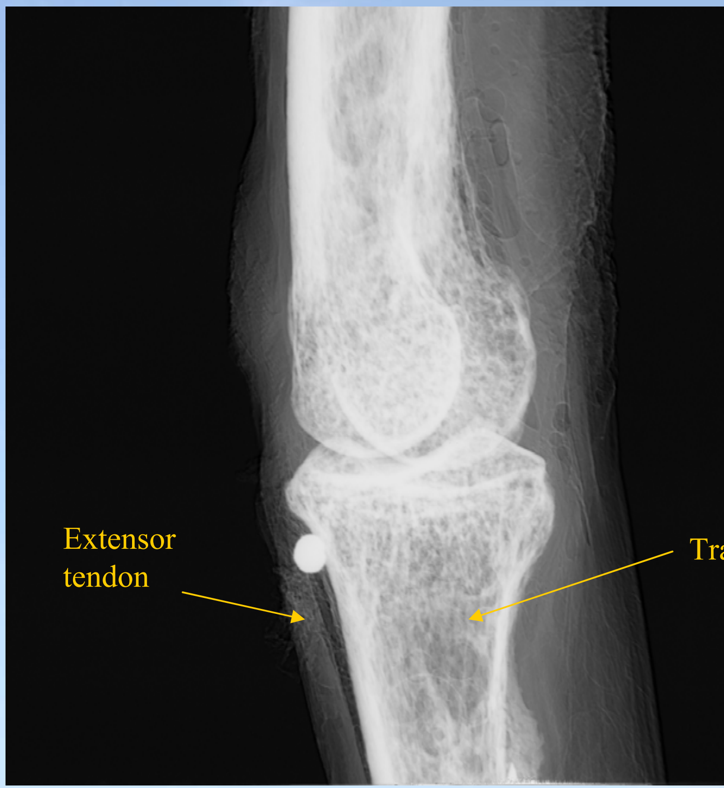

Apparent absorption Image

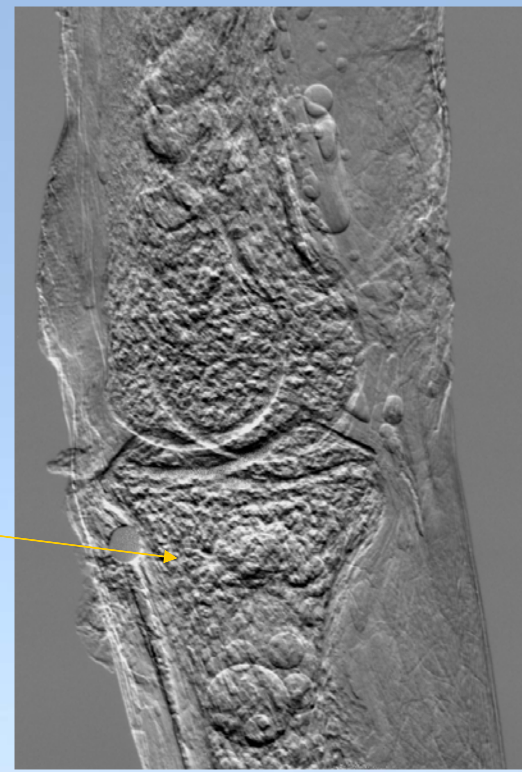

Refraction Image

Index finger proximal interphalangeal joint

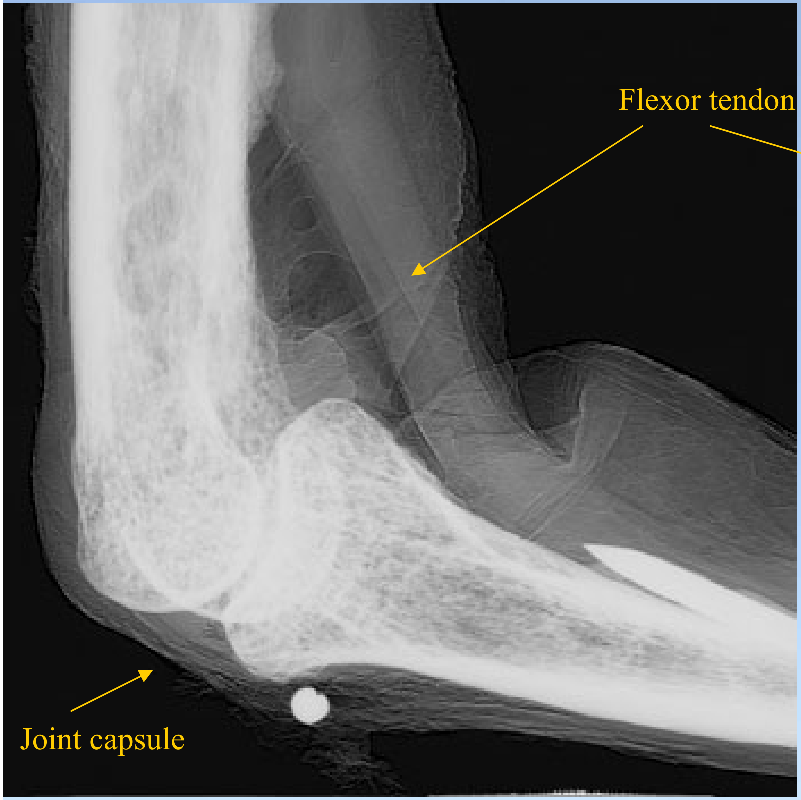

Apparent absorption Image

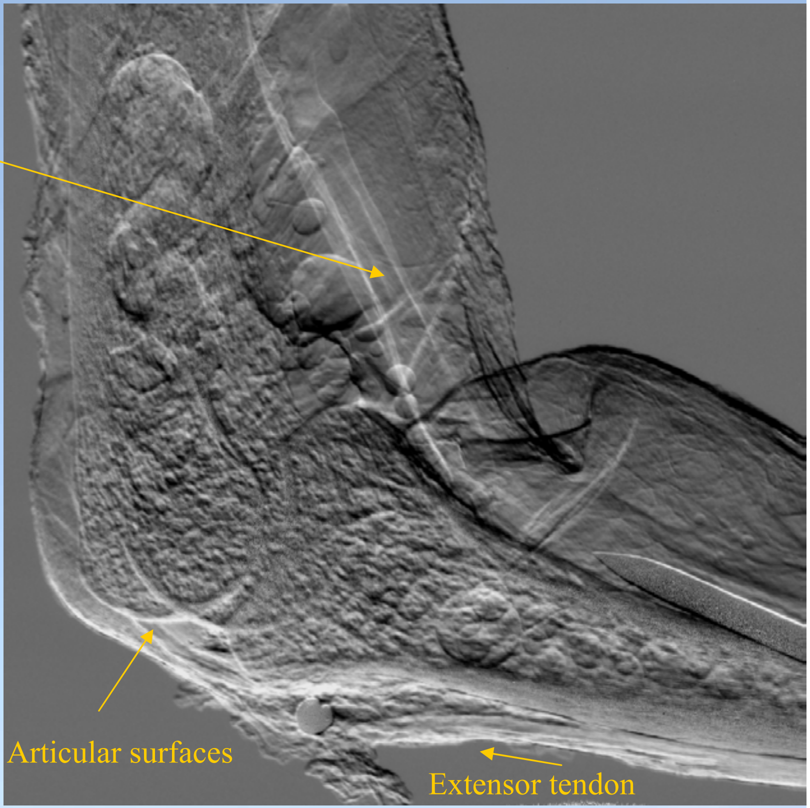

Refraction Image

Computed μ-Tomography (μ - CT)

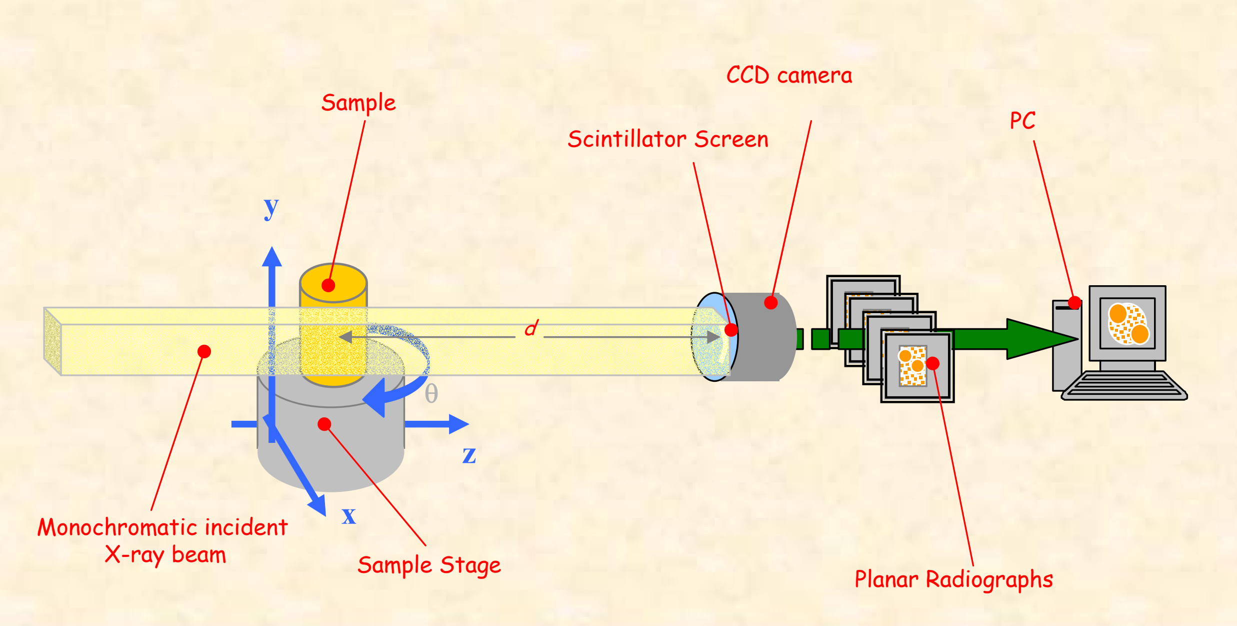

- μ -CT allows to investigate the **internal features** of a sample **without sectioning** it:
  - → in many cases the **sectioning procedure** modifies the sample structure
  - → the sample can be after **studied by other** experimental **techniques**,
  - → or submitted to several **treatments** (mechanical, thermal, etc...)

Study of trabecular bone structure

- In the adult there are two main types of bones: the cancellous (trabecular) and the compact one. The first is mainly involved in the metabolic processes of calcium homeostasis while the second has principally the mechanical function of support.
- Osteoporosis causes alterations in the trabecular bone that produce a reduction of bone mass but also by structural changes in the bone architecture.
- Bone mineral density is often estimated in vivo using Dual Energy X-ray Absorptiometry which evaluates the mineral contenent of bone.
- The quantification of bone microarchitecture is mainly based on histology that allows to extract histomorphometric parameters quantifying bone structure in terms of shape and connectivity. This techique is destructive.

Absorption microtomography: Trabecular bone structure

Elastic properties of bones are determined by: composition, density and bone architecture.

E= 26 keV
Absorption radiograph

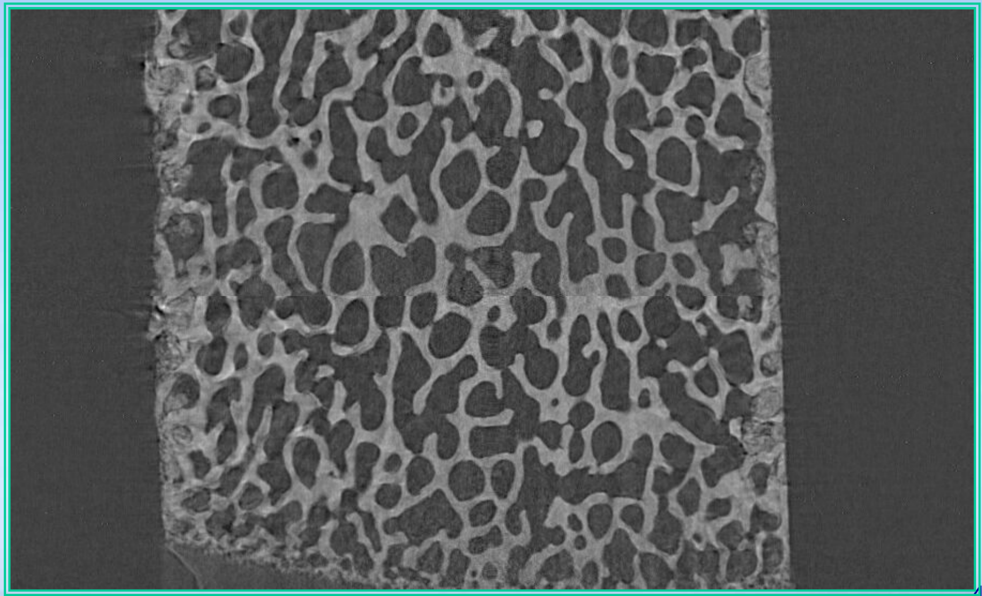

E= 26 keV
Absorption tomograph

Samples by: D.Dreossi, F.Vittur, F.Cosmi
University of Trieste

Reconstructed volume from a sample of pig trabecular bone

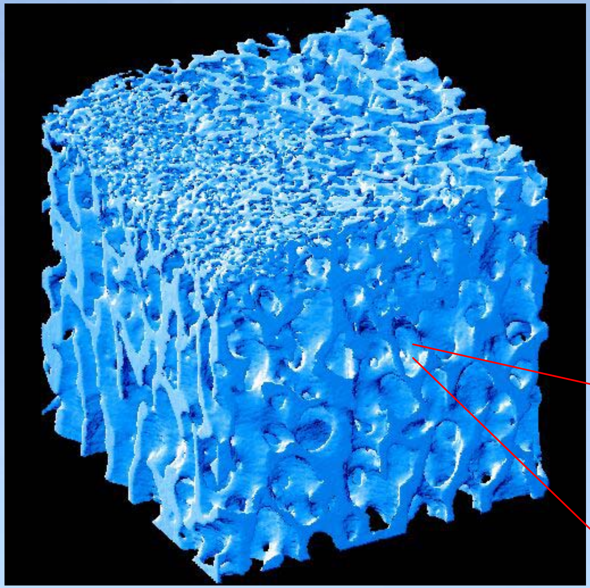

224 pixels voxel

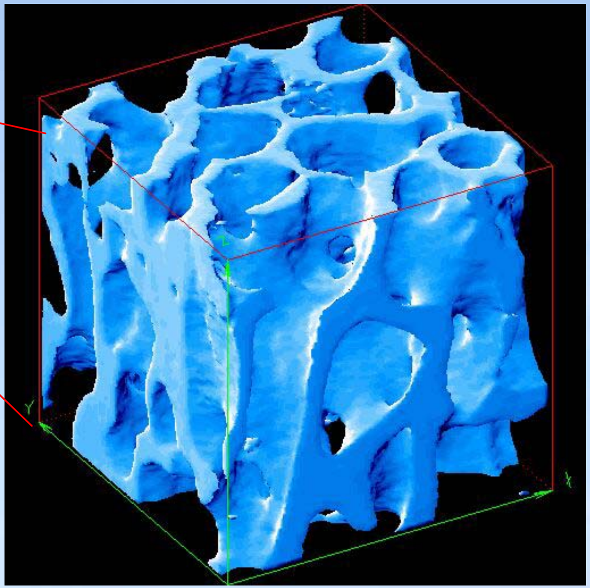

100 pixels voxel

High resolution μ-CT analysis of a proximal human femur with an innovative linear detector

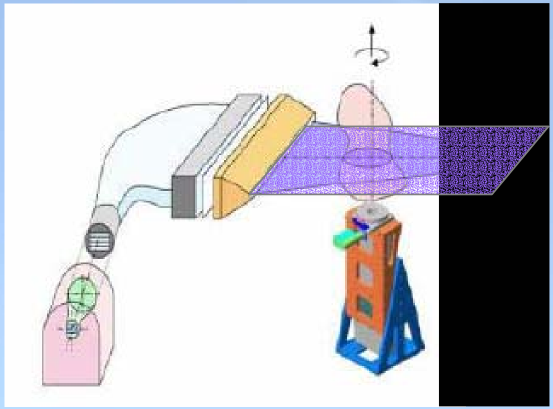

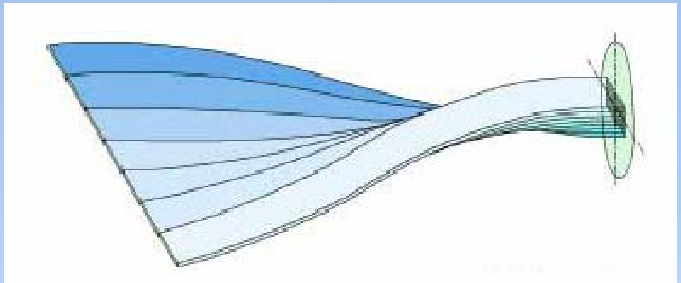

- Investigation of the **performance of a EBCCD-based system** with a nominal spatial resolution of 22.5 μm extended over a **FOV of 130 mm x 1 mm**.
- This system is obtained by using **a distinctive fiberoptic ribbon** (patented by the **University of Bologna**) converting a linear geometry to a rectangular one.
- A scan of **a 9 cm wide human proximal femur** allowed to analyze the trabecular structure of the bone in order to investigate changes caused by **osteoporosis**.

A. Pasini et al., Proceedings of IEEE NSS/MIC 2004 Annual meeting, Rome, Italy

10 cm

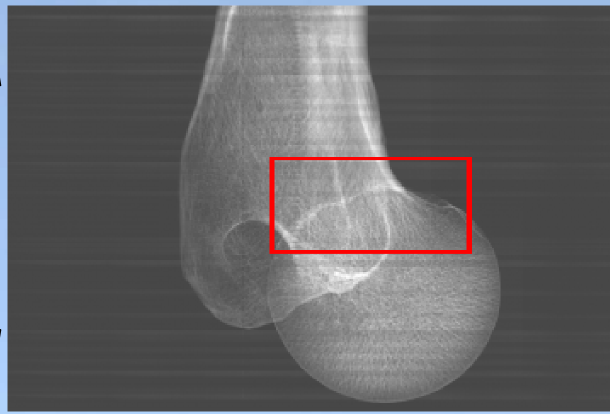

E = 34 keV

t_{exp} = 600 sec

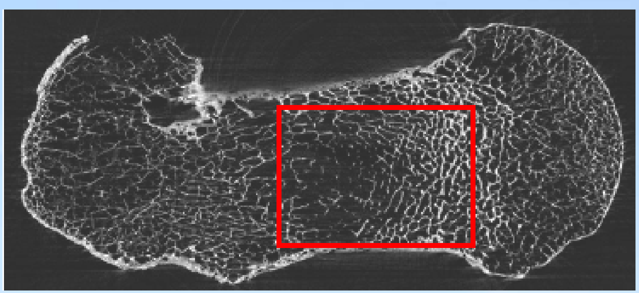

Reconstructed slice

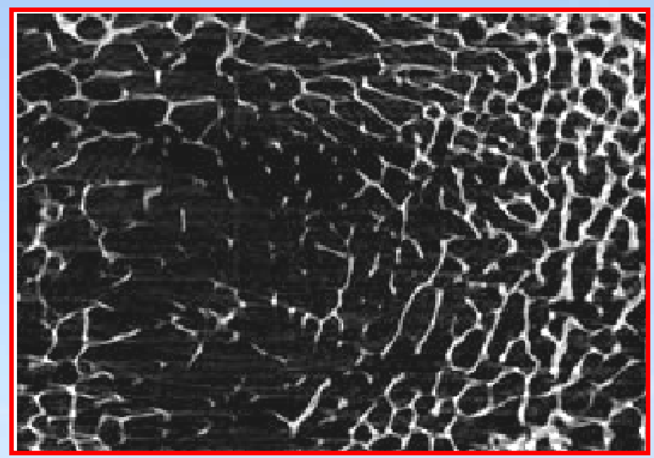

A. Pasini et al., Proceedings of IEEE NSS/MIC 2004 Annual meeting, Rome, Italy

Rendering of 50 slices

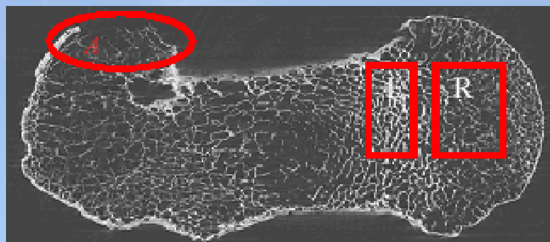

	BV/TV [%]	Tb.Th [μm]	Tb.N [mm^{-1}]	Tb.Sp [μm]
Left ROI	21.4±0.3	167±2	1.28±0.03	610±20
Right ROI	13.8±0.2	120±1	1.17±0.02	740±10

	BV/TV [%]	Tb.Th [μm]	Tb.N [mm^{-1}]	Tb.Sp [μm]
Big ROI	17.5±0.2	122±2	1.44±0.02	576±8

LEGENDA:
BV/TV – Bone Volume/Tissue Volume
Tb.Th – Trabecular thickness
Tb.N – Trabecular Number
Tb.Sp – Trabecular Space

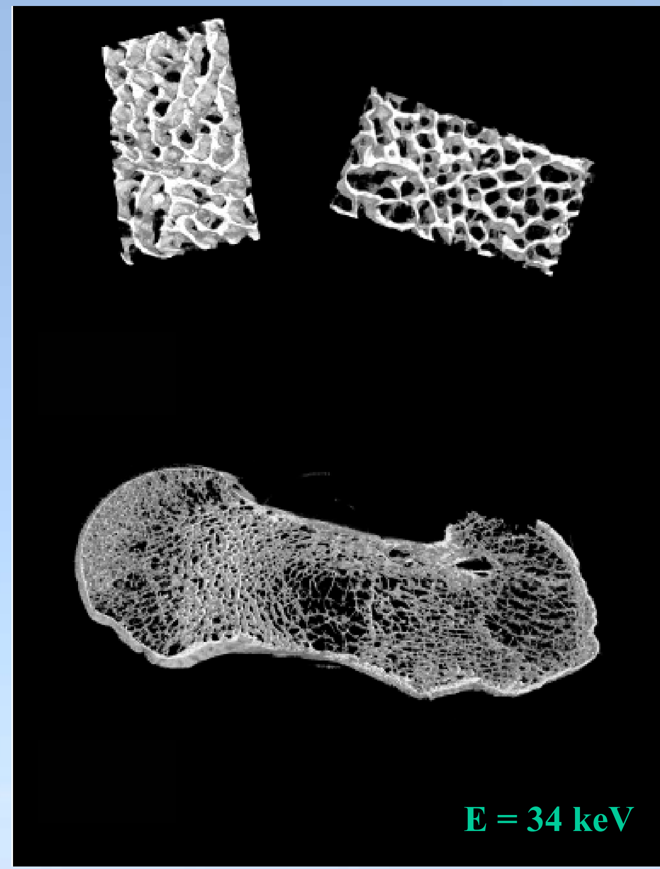

Study of the bone structure adjacent to oral implants

- One of the most important aims about **cortical and cancellous bone** researches is to understand the factors that determine their **mechanical properties**, how these properties are maintained, and how bone reacts to changes in its environment, such as the introduction of a **Ti implant**.

- **Trabecular morphometry** has been traditionally assessed in **2D**. Particularly limiting is the **destructive** nature of this extremely time consuming procedure. Synchrotron radiation **X-ray microtomography** allows to investigate the **3D microstructure** of bone.

- Beam energies between 30 and 40 keV will provide **a satisfactory signal-to noise ratio** and contrast for the bone, except for the parts falling in the shadow of the Ti screw. Then, we investigated the effect of **Al implants**.

L. Tesei, F. Casseler, D. Dreossi, F. Zanini, L. Mancini, G. Tromba

Reconstructed slice obtained at the ESRF

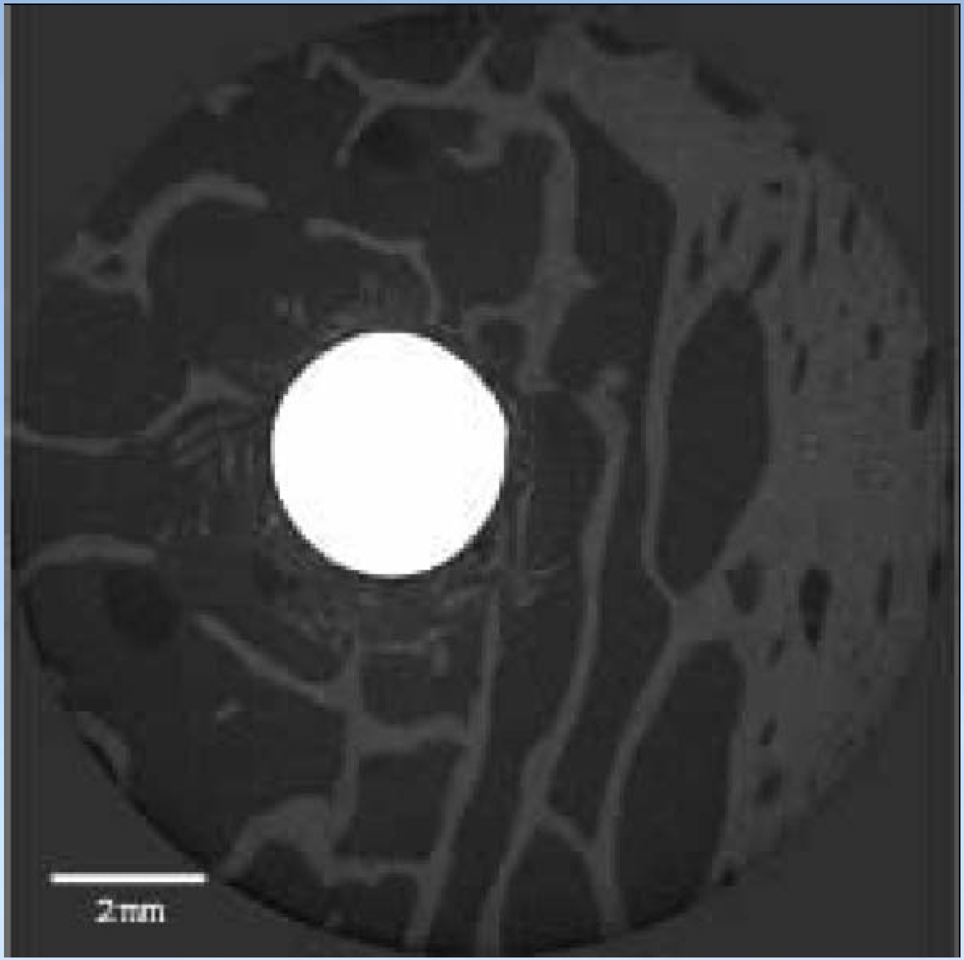

E = 50 keV

L. Tesei et al., NIM A, 548 (2005) 257-263

Comparison before and after the bone implant

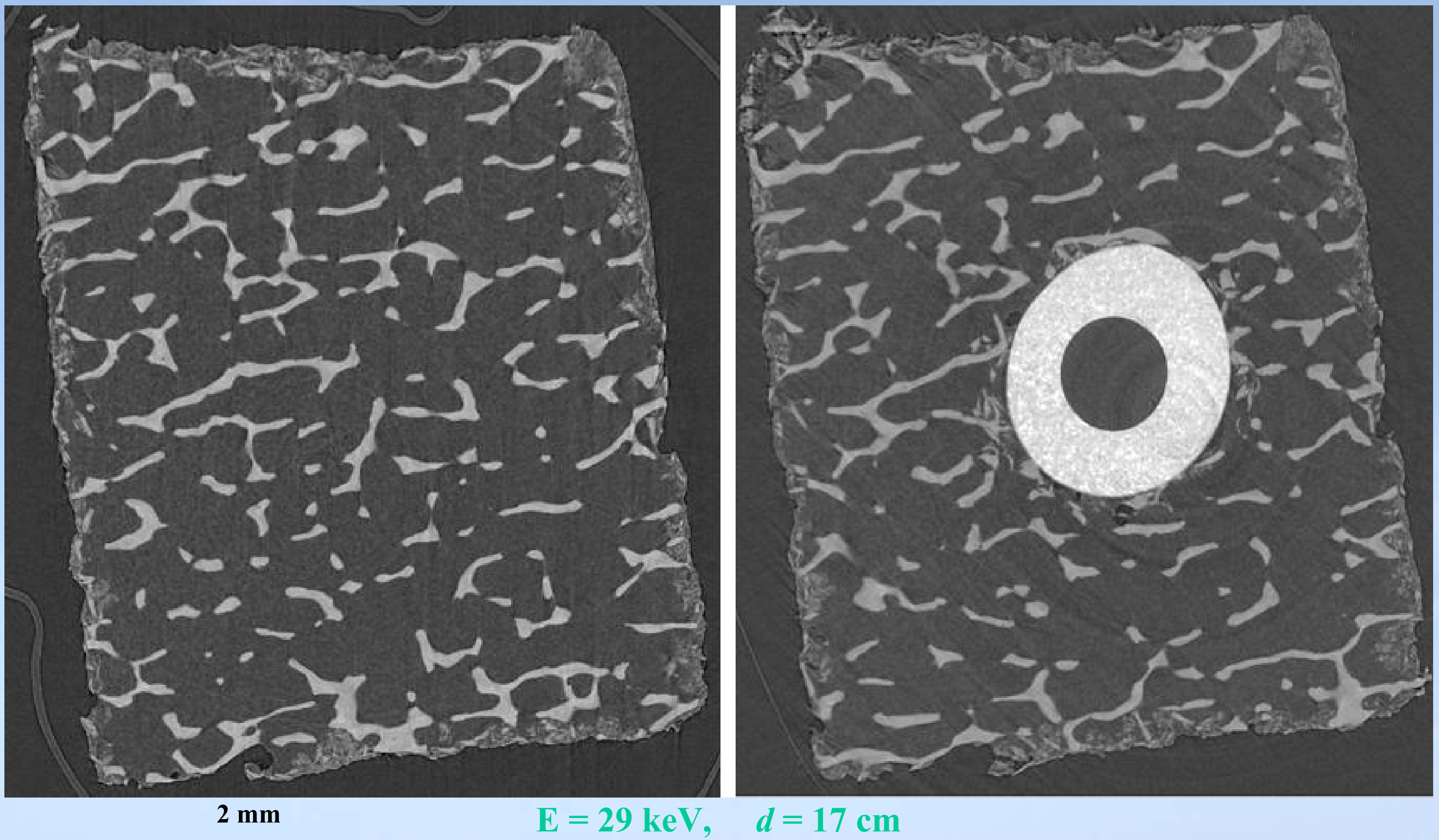

E = 29 keV, *d* = 17 cm

L. Tesei et al., NIM A, 548 (2005) 257-263

Study of the bone damage around the implant

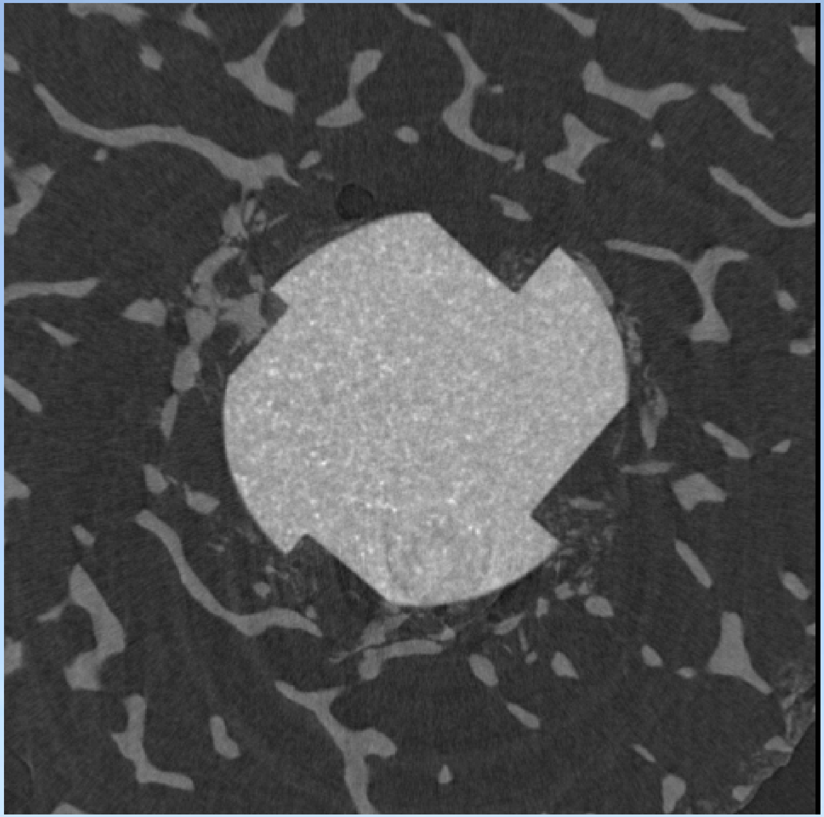

Screw: ∅ 3mm, anchorage length 8.5 mm

1 mm

E = 29 keV, *d* = 17 cm

L. Tesei et al., NIM A, 548 (2005) 257-263

3D rendering of the implanted bone

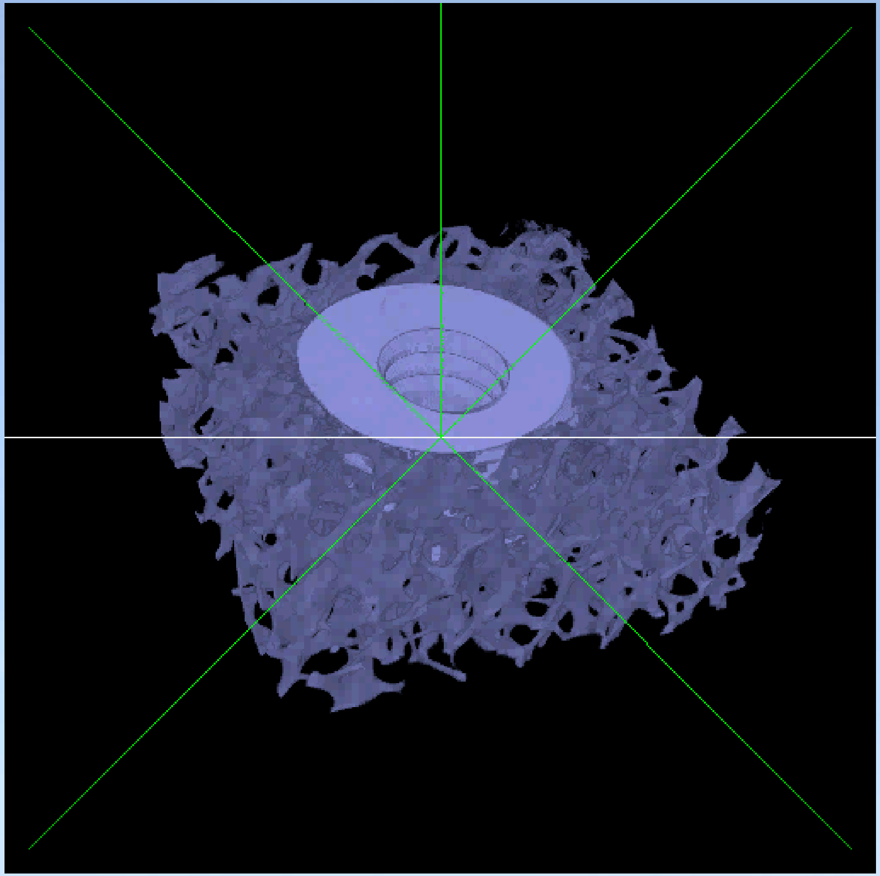

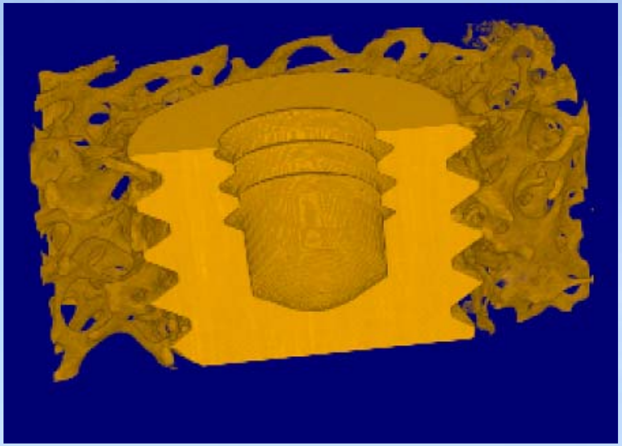

1 mm

E = 29 keV, *d* = 17 cm

L. Tesei et al., NIM A, 548 (2005) 257-263

PHC and K-edge imaging: Mapping of the metal intake in plants by X-ray micro-radiography and tomography

- **Accumulation of metals**, such as **Cu, Zn, As, Cd, Pb, Hg**, **in the environment** is a high health risk because of the possibility for these elements to be transferred to living organisms through fresh water or vegetables.

- **Among the different solutions**, a very **promising method** is **phytoremediation**: it consists in the removal of contaminants by means of their absorption and accumulation in roots and leaves of plants, specially cultivated for this purpose and then harvested. Recently, also transgenic plants have been obtained, with higher accumulation properties.

To study these problems: detection of contaminants, comparison of accumulation properties of the various plants, mapping of possible biological structures accumulating specific metals within a tissue.

- We used **dual-energy micro-radiography** taking advantage of the highly-monochromatic, large-field synchrotron radiation to detect the heavy-metal accumulation in 2D and 3D biological samples.

J. Kaiser et al., Eur. Phys. J. D 32, 113–118 (2005)

Pb detection by dual energy imaging in Helianthus annuus leaf

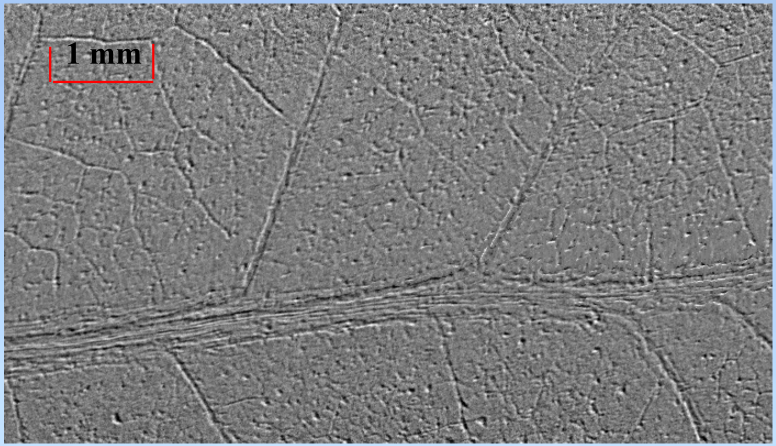

10 mM $PbSO_4$ treated sample

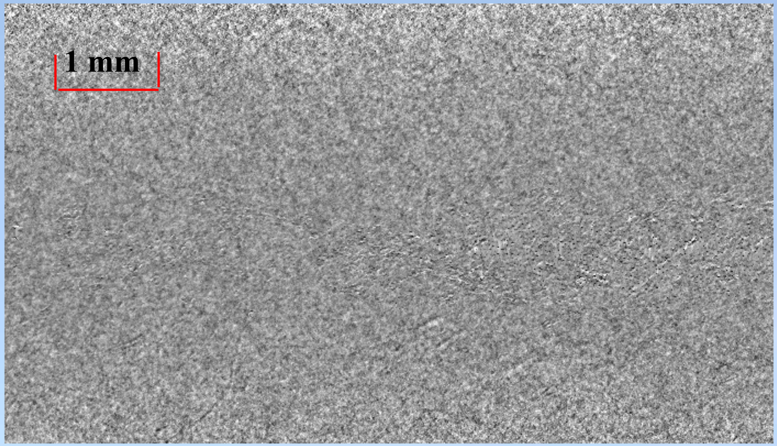

Untreated control sample

E = 13.150 and 12.975 keV

D =168cm

J. Kaiser et al., Eur. Phys. J. D 32, 113–118 (2005)

Cu detection by dual energy imaging in Phaseolus vulgaris leaf

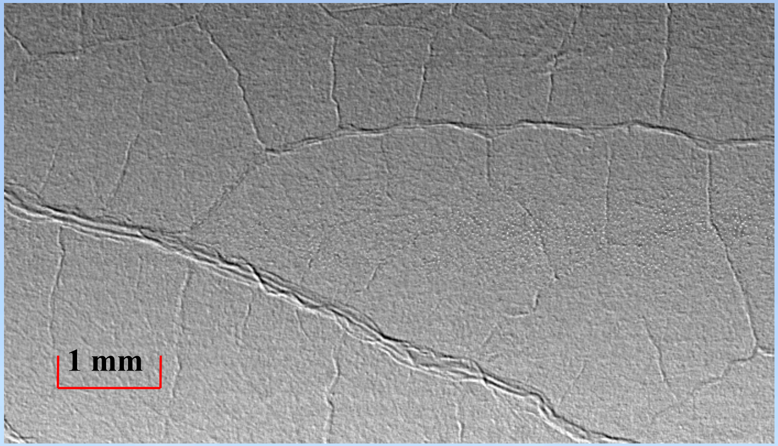

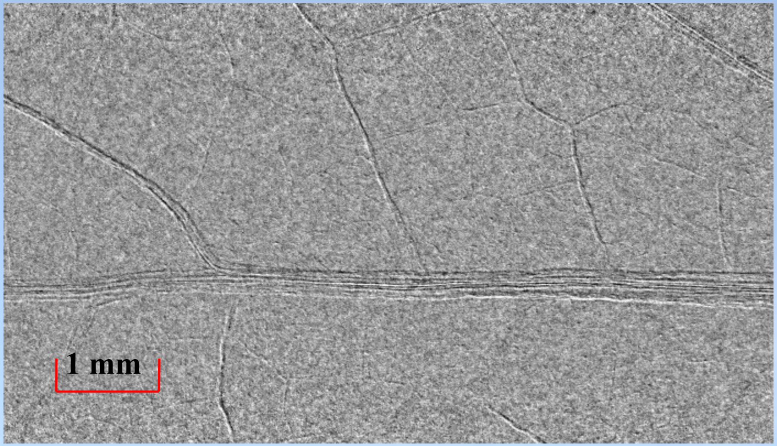

15 days 10 mM $CuSO_4$ treated samples: ethanol-fixed compared with air dried

E = 9.05 and 8.90 keV

***d* = 35 cm**

J. Kaiser et al., Eur. Phys. J. D 32, 113–118 (2005)

Cu detection by dual energy imaging in Phaseolus vulgaris leaf

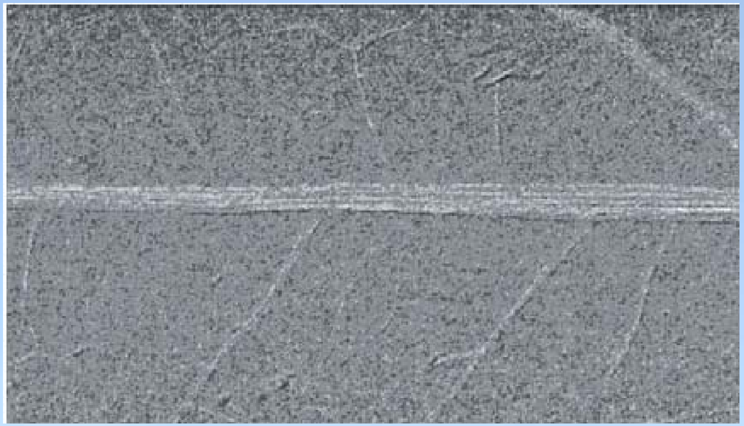

15 days 10 mM $CuSO_4$ treated samples: ethanol-fixed compared with air dried

E = 9.05 and 8.90 keV

***d* = 2 cm**

J. Kaiser et al., Eur. Phys. J. D 32, 113–118 (2005)

Cu detection by dual energy imaging in *Phaseolus vulgaris* leaf

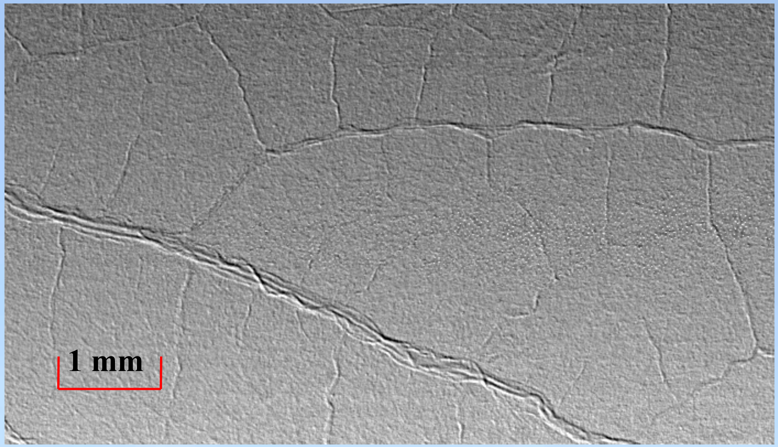

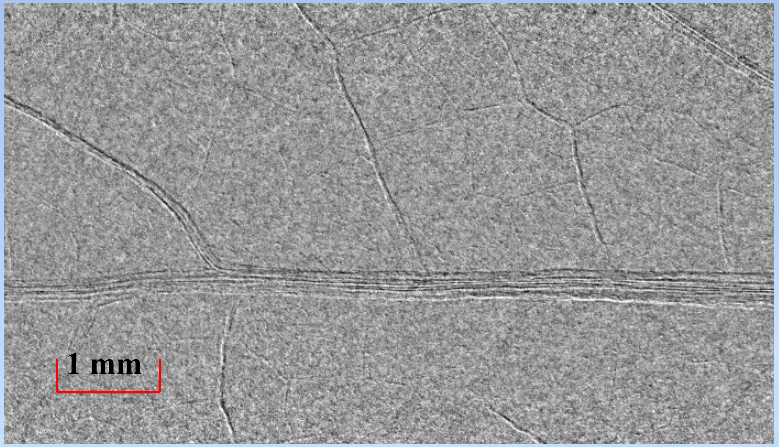

15 days 10 mM $CuSO_4$ treated samples: ethanol-fixed compared with air dried

E = 9.05 and 8.90 keV

d **= 35 cm**

***J**. Kaiser et al., Eur. Phys. J. D 32, 113–118 (2005)*

Mapping of the metal intake in plants by dual energy μ-CT

Dyplotaxis erucoides root grown in 2% $CuSO_4$ solution

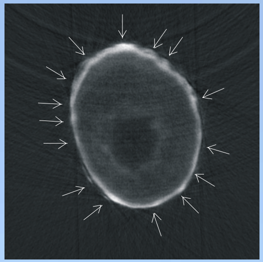

difference

E = 9.05 and 8.90 keV

h = 1 mm
∅ ca. 3 mm

3D rendering

Helianthuus annuus leaf treated in a 10 mM $PbSO_4$ solution

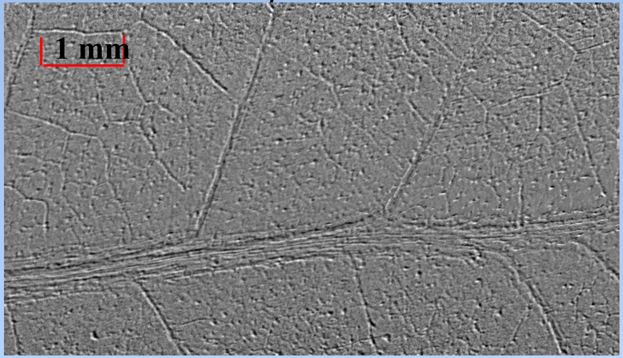

E = 13.150 and 12.975 keV

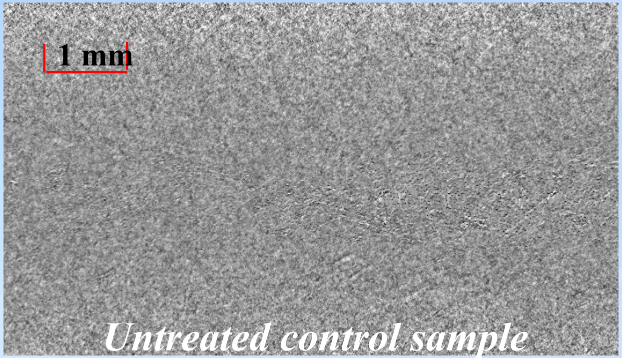

J. Kaiser et al., Eur. Phys. J. D 32, 113–118 (2005)

Archeological glasses

- Glasses develop corrosion layers during exposure to different environmental conditions. This process changes the surface morphology and its chemical composition. In extreme cases, the whole fragment is corroded. These pieces are extremely fragile and require special conservation treatments.

- The effectiveness of polymers used for glass consolidation depends on the penetration of organic material in porous inorganic substrate. The detection of polymers in corroded layers is a special problem in conservation research.

- Recognized methods of analysis require embedding in a polymer to prepare cross sections (SEM) or sputtering (depth profiles). Need for a non-destructive technique.

H. Roemich, S. Gerlach, E. López F. Zanini, L. Mancini, L. Rigon

Original waterlogged glass, completely corroded
Fragment provided by the Museum of London

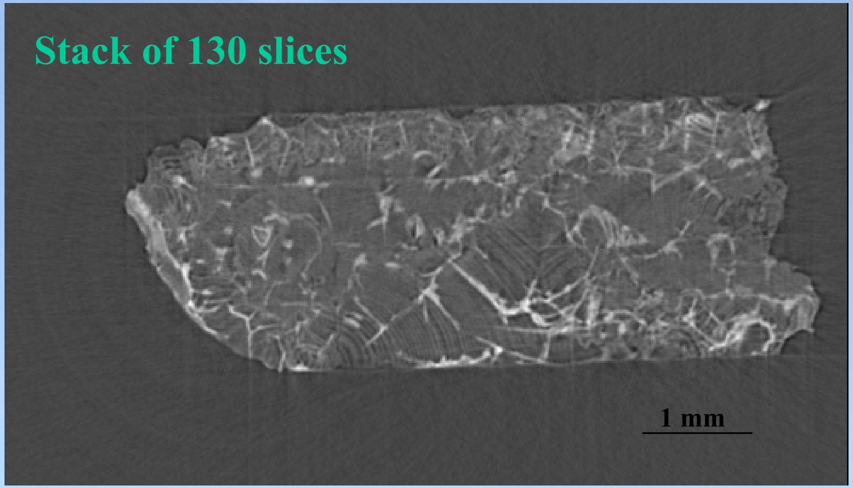

E = 25 keV   *d* = 66 cm; *acquisition time: 4h*

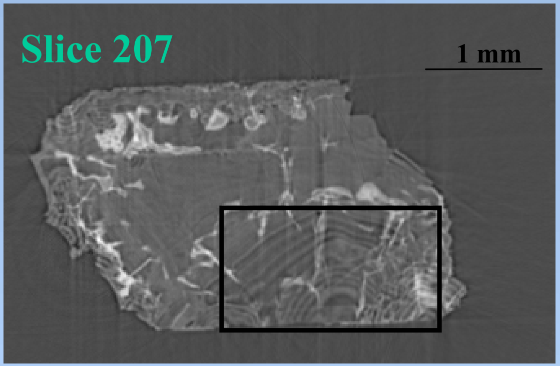

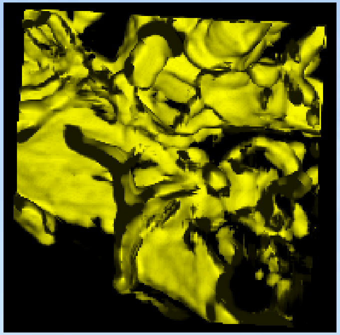

Cine rendering of channels
(9.0 x 9.0 x 0.2) mm^3

It is possible to visualize:

→ the gel-layer channels

→ the lamellar structure inside the corroded glass

Gerlach S. et al., Elettra Highlights 2003, 80

Model glasses covered by a polymeric layer
Bulk polymers (acrylates) are used as consolidant materials

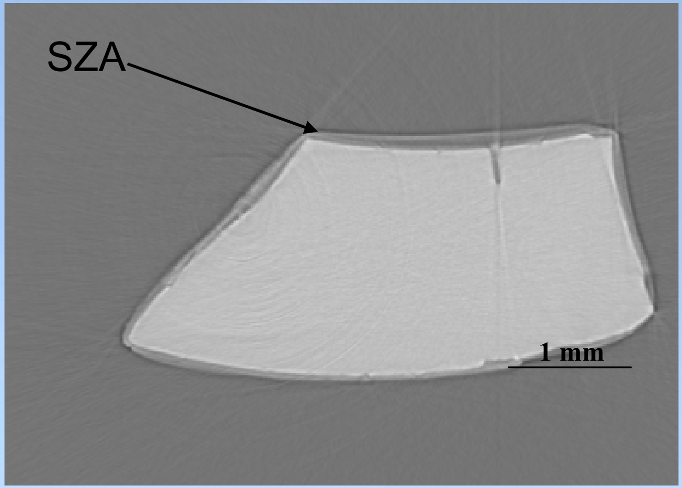

Inorganic layer based on Silicium-Zirconium-Alcoxides (SZA) well visible on the glass surfaceS. SZA penetrates the crack on the upper surface. The channel is completely filled without formation of voids.

E = 25 keV, *d* = 66 cm

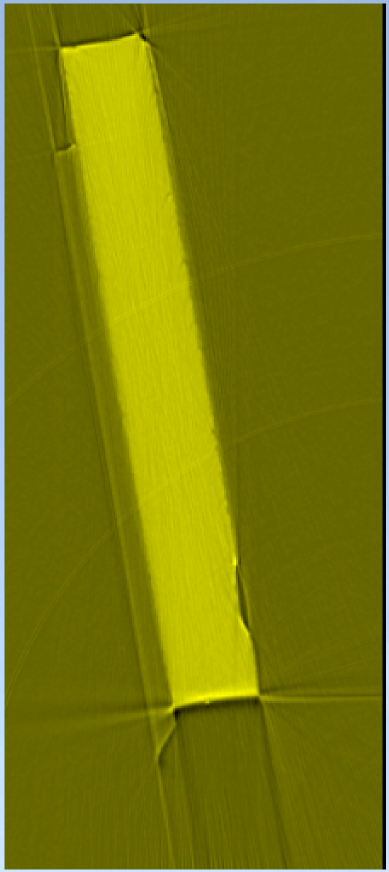

A 200 μm layer of Araldite well visible

Gerlach S. et al., Elettra Highlights 2003, 80

Densitometrical study of waterlogged archeological wood (AW)

- **Waterlogged AW**: refers to wood excavated from different types of archeological sites. The time in which wood has been waterlogged is considerably long, often over than one thousand years.

- Main characteristics completely different from original wood: the **environmental condition** is the reason of a so long conservation, but water has caused the physical and chemical degradation. The different conservation's sites (type of water, soil composition, etc.) might determinate completely different condition of degradation.

- The **specific objective**: to have a measurement of the linear attenuation coefficient of AW's cell wall and then it can be compared with the value of the linear attenuation coefficient of the same species but not degraded. Then, the grade of degradation of cell walls could be determined **with a not severe destructive method**.

Reconstructed slice with three AW samples

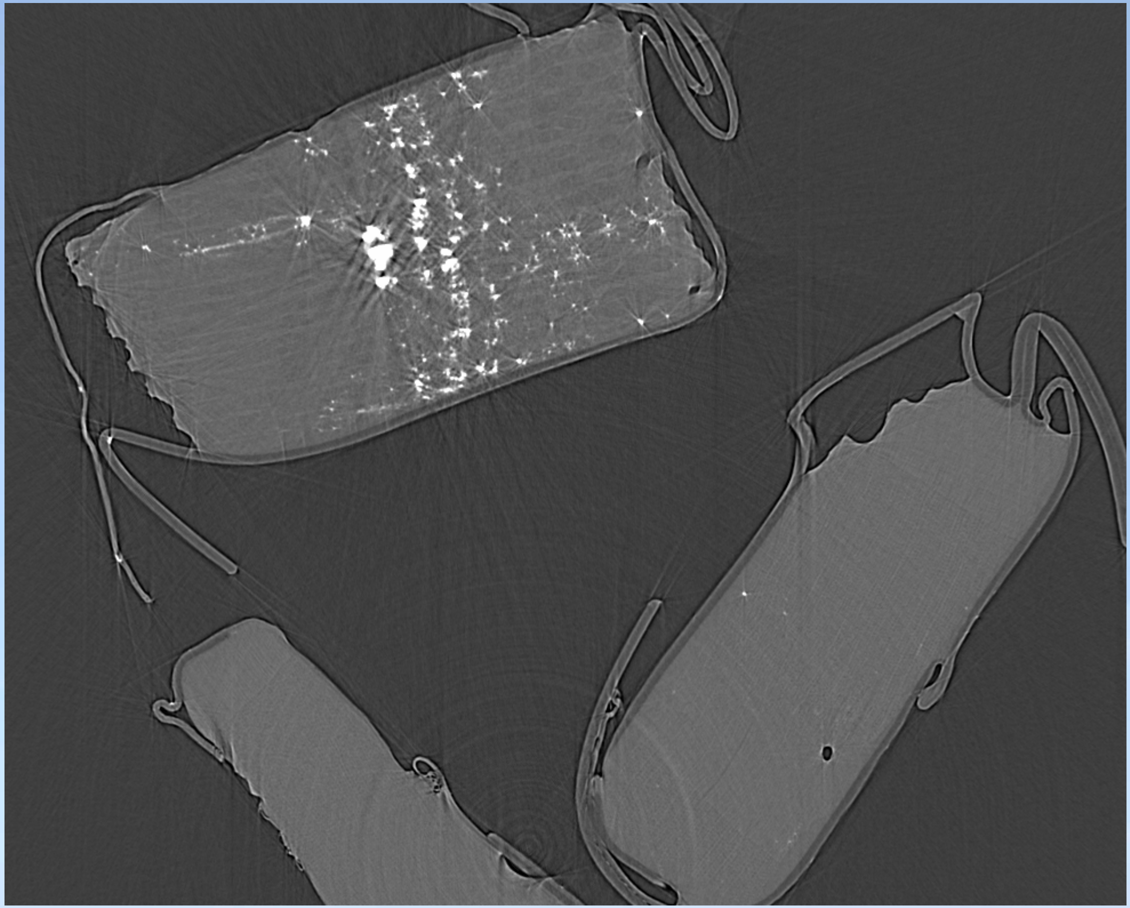

E = 17 keV, *d* = 20 cm

Quercuus samples: μ–CT vs. Optical Microscopy (OM)

OM

Recent sample

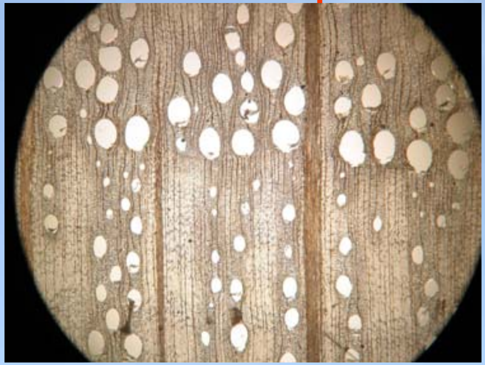

Archeological sample

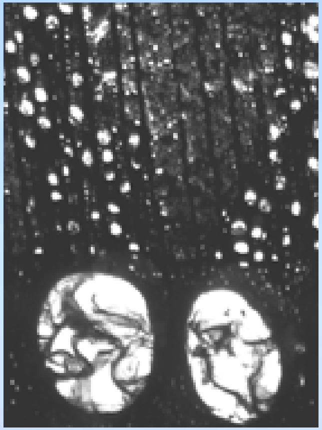

μ-CT

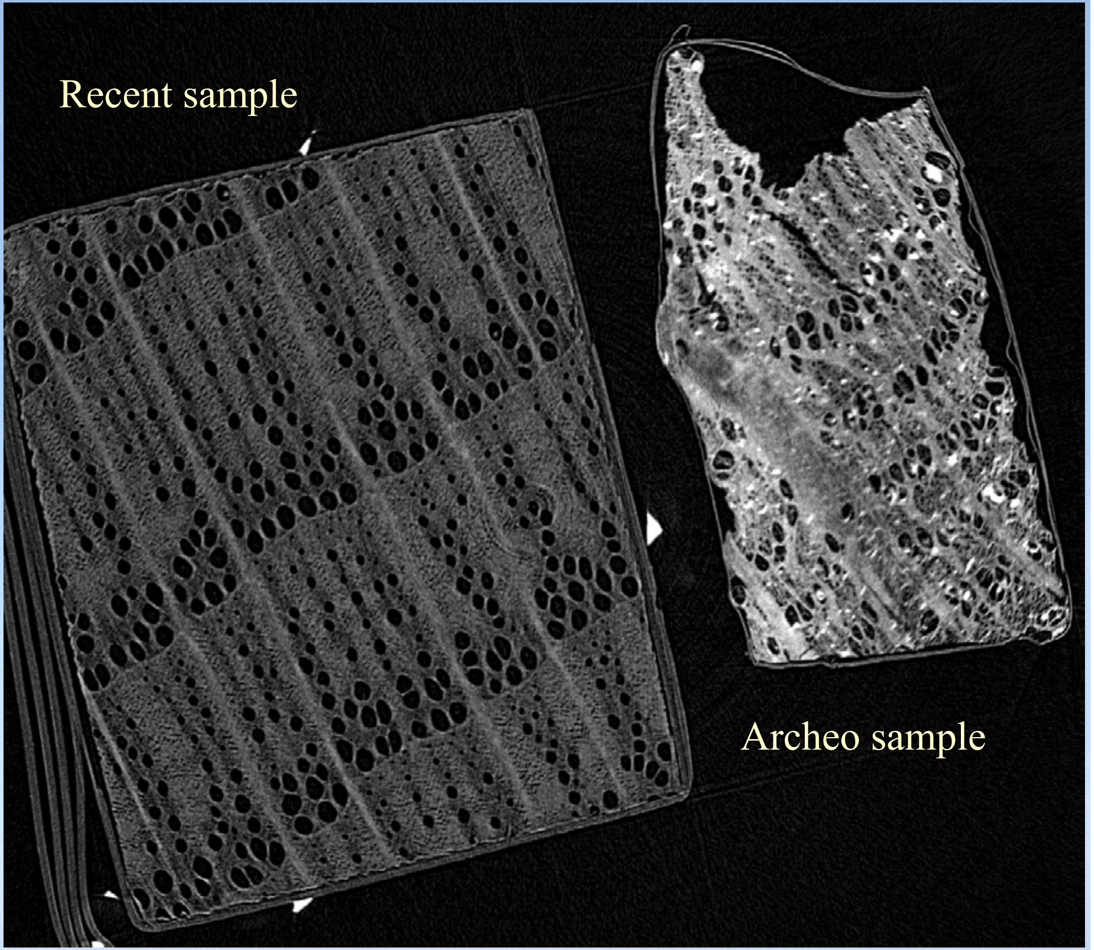

Acknowledgement

to the SYRMEP team:

L.Mancini, R.H. Menk, F.Zanini: Sincrotrone Trieste
L.Rigon: Sincrotrone Trieste and ICTP
F.Arfelli, E.Castelli, D.Dreossi, R.Longo: Università di Trieste e INFN

.... to the beamline users who contributed with their experiments:

F.Casali et al.: Università di Bologna
Fioravanti, N.Sodini: Università di Firenze
C.Hall et al.: Daresbury laboratory
S.Evans, Royal Marsden Hospital, London
Alan Hufton, Christie Hospital, Manchester
J.Kaiser et al., Univ. of Brno, Università dell'Aquila
S. Majumdar et al, University of California
F.Cosmi, M.Maglione, F.Vittur, Università di Trieste
R.Lewis et al.,Monash University, Melburne
Römich, S. Gerlach, Fraunhofer Institute, Bronnbach-Branch
L.Tesei, I. Teseo Tesei Trieste
S.Wilkins, CSIRO, Melburne